



Evaluating the influence of meteorite impact events on global potassium feldspar availability to the atmosphere since 600 Ma

B. C. Coldwell^{1,2} & M. J. Pankhurst^{1,2,3,4,5*}

¹ Instituto Tecnológico y de Energías Renovables (ITER), 38600 Granadilla de Abona, Santa Cruz de Tenerife, Spain

² Instituto Volcanológico de Canarias (INVOLCAN), Calle Álvaro Martín Díaz 1, 38320 San Cristóbal de La Laguna, Santa Cruz de Tenerife, Spain

³ School of Materials, University of Manchester, Manchester M13 9PJ, UK

⁴ Research Complex at Harwell, Harwell Campus, Didcot OX11 0FA, UK

⁵ School of Earth and Environment, University of Leeds, Leeds LS2 9JT, UK

B.C.C., 0000-0001-9240-6240; M.J.P., 0000-0001-6844-9822

*Correspondence: mpankhurst@iter.es



Abstract: Potassium feldspar present in global mineral aerosol (<5%) plays a disproportionate role in modulating the microphysics of mixed-phase cloud. Via exceptional ice nucleation properties, it is capable of changing cloud properties and behaviour. Here we identify times of substantial and abrupt change in the global availability of potassium feldspar since 600 Ma. Normally, weathering and vegetation cover contribute to low availability, with clay dominating mineral aerosol. Periods of maximum availability are reasoned to follow the emplacement and remobilization of ejecta blankets from major meteorite impact events, before returning to background after some hundreds to thousands of years. We review the 44 largest confirmed craters and evaluate the potassium feldspar content of their target rocks, which range from c. 0 to >30%. By combining crater size and tectonic reconstructions, we are able to provide a quantitative and self-consistent assessment of changes to global potassium feldspar availability. Considerable differences in potassium feldspar availability following meteorite impact events are revealed. Different impact events generated dust containing different amounts of potassium feldspar. Differing levels of influence upon climate are hypothesized, and should now be tested by looking at stratigraphic records of these events to reveal the sensitivity of climate to different dust mineralogy.

Supplementary material: Figures showing palaeolatitude determinations using various methods and reconstruction models, and estimates of alkali feldspar abundance and distribution across contemporary continental landmasses for meteorite impact events are available at: <https://doi.org/10.6084/m9.figshare.c.4253312>

Received 24 April 2018; revised 2 October 2018; accepted 3 October 2018

Cloud dominates albedo and controls the distribution of water and sunshine across the Earth. Even subtle changes to cloud influence the wider Earth system. For example, sub-per cent per year changes in cloud cover over Greenland control the mass of its ice sheet by mediating the primary addition rate (Hofer *et al.* 2017). Variations in optical properties and behaviour of cloud are integral to weather, the hydrological cycle and climate, yet they remain difficult to parameterize and predict (Tan *et al.* 2016; Storelvmo 2017; Xie *et al.* 2017).

Ice nucleation is a microphysical process that dramatically changes optical properties (brightness, affecting radiative transfer) and behaviour (shortens lifetime by promoting rain) of cloud (Lohmann & Feichter 2005; Hoose & Möhler 2012). Whereas liquid water can supercool to -35°C in the atmosphere, ice formation is triggered at much warmer temperatures on the surfaces of aerosols acting as ice nucleating particles, INPs (Murray *et al.* 2012; Nenes *et al.* 2014; Herbert *et al.* 2015; Vali *et al.* 2015; Koop & Murray 2016). The amount of INPs in the atmosphere is critical to cloud behaviour and climate (Vergara-Temprado *et al.* 2018), as is the efficiency of those INPs.

Mineral dust accounts for around half the total aerosols in the modern atmosphere (Textor *et al.* 2006). This aerosol is composed mainly of clay (Atkinson *et al.* 2013) emitted from arid areas of the Earth (Gieré & Querol 2010). Mineral aerosol has been found to account for a large proportion of all ice nuclei in Earth's modern atmosphere, yet clay is poor at nucleating ice (Atkinson *et al.* 2013). In the past 5 years, research first identified feldspar as having

exceptional ice nucleating properties (Atkinson *et al.* 2013). Further investigation revealed that only the alkali feldspars, not plagioclase, exhibit these properties (Zolles *et al.* 2015; Harrison *et al.* 2016; Peckhaus *et al.* 2016).

Of the alkali feldspars (Afs; mineral abbreviations from Siivola & Schmid (2007) and Whitney & Evans (2010) are used throughout), more potassic samples appeared, overall, to be better at nucleating ice than sodic (Harrison *et al.* 2016). Recently, an explanation as to why has been reported by Whale *et al.* (2017): the most efficient Afs are those that exhibit perthitic texture whose nanoscale topography, which includes etch pits and tunnels as a result of solution-feldspar reactions, probably acts to promote ice nucleation by providing suitable settings at the scale of a critical ice nucleus (the minimum cluster size of water molecules required for the spontaneous growth of ice) (Whale *et al.* 2017). Perthite is potassium feldspar (Kfs) with exsolved albite (Ab) lamellae, and is prevalent in granitic rock types (see Parsons *et al.* (2015), to whom we direct the reader for a recent review of alkali feldspar microtextures). Consequently, Afs, and particularly perthitic Kfs, is considered to play a role in the global atmospheric and hydrological cycle that is highly disproportionate to its abundance. It is therefore Kfs that we focus our attention upon here.

Although laboratory-derived knowledge of specific mineral ice nucleation is growing (see Kiselev *et al.* 2017; Whale *et al.* 2017), determining real effects is challenging (Storelvmo 2017). This is partly because cloud properties are difficult to measure directly in real time (Tan *et al.* 2016). Furthermore, cloud properties are impossible to measure, at least directly, in the deep past.

Knowledge of the abundance and type of aerosols in the past is therefore important to improving understanding of modern and future atmosphere dynamics (see Buseck & Pósfai 1999; Andreae 2007), because it is the indirect effects of aerosols (i.e. via changes to cloud properties and behaviour; Komurec *et al.* 2014) that contribute the largest uncertainties in global climate models (Stocker 2014). Currently, baseline knowledge concerning pre-industrial aerosols is poor (Carslaw *et al.* 2017).

Is a proxy record of ice nucleation regime possible?

Pankhurst (2017) provided an Earth-history scale overview of the availability of potassium feldspar (Kfs), to form the first step towards such a proxy record for an ice nucleation regime. No attempt was made to review mineral texture, or chemistry, as more work is required to determine links between ice nucleation efficiency, chemistry and texture of the feldspar group. It was simply reasoned that formation of granite and even more potassic intrusive and metamorphic equivalents (syenite, alkali feldspar granite, gneiss) fundamentally controls Kfs crustal distribution on a global scale, and that this lends the widest possible context for future study of links between mineral dust and cloud in the past.

Key points from Pankhurst (2017) include the following: (1) the accumulation of granites during construction and evolution of continental crust has increased Kfs primary availability, yet processes such as soil formation (feldspar to clay) and changing vegetative or ice cover probably play a more important role in modulating how much Kfs is able to be aerosolized on shorter timescales; (2) it is demonstrated that the availability of Kfs and its contribution to aerosol has not been constant across the averaged Earth's surface in time; (3) dust leaves a physical record (e.g. loess and other aeolian deposits) in which mineralogy can be measured; (4) a Kfs factor (KFF), which is simply the volumetric per cent abundance (i.e. pure Kfs has a KFF of 100), can be assigned to atmospheric dust, current land surfaces, rocks and aeolian deposits, which provides a shorthand nomenclature for linking multidisciplinary study.

Climate forcers such as pCO₂ (Booth *et al.* 2017) and sulphate aerosol (Langmann 2014) have records composed of both historical measurements and often much longer term proxies (Booth *et al.* 2017; Wolfe *et al.* 2017). When linked to effects via laboratory-derived understanding and natural evidence, such proxy records provide the basis for model validation (Schmidt *et al.* 2011; Booth *et al.* 2017). Because the origins of dust in today's atmosphere can be fingerprinted to specific regions (Zhao *et al.* 2018), and a KFF can be derived from each (Pankhurst 2017), it becomes possible to make predictions about the effects of specific mineral dust events.

However, if the importance of Kfs to cloud behaviour is to be addressed with the aid of a pre-industrial and potentially much longer proxy record, what is needed first is to identify the best possible time periods in the rock record for multidisciplinary study. Owing to the low concentration of aerosol particles under pre-industrial conditions, global mean cloud albedo during much of Earth history could have been twice as sensitive to changes in aerosol emission as it is today (Carslaw *et al.* 2017). As such, any effects of changing mineral aerosol volume or variety may be more pronounced, and therefore evident.

Targeting the largest dust-refreshing events through time

The mineralogy of dust sources varies considerably across the planet (e.g. Scheuvens *et al.* 2013; Smith *et al.* 2014), yet in normal circumstances clay minerals dominate the global mineral aerosol budget (Atkinson *et al.* 2013) owing to the continual process of chemical weathering (White *et al.* 2001). Weathering (i.e. from feldspars to clays) forms a thin barrier between 'fresh rock' and

'fresh air'. This regime has been in place since at least the Neoproterozoic (Eriksson *et al.* 2013), and is reasoned to both suppress and buffer mixed-phase cloud ice-nucleation efficiency in the Earth system (Pankhurst 2017). Changing this regime requires fresh minerals to cover the clay barrier, and therefore be available to become aerosolized. To affect global aerosol mineralogy, this natural barrier must be overcome rapidly and dramatically.

Meteorite impact events do just this. The rock and mineral fragments excavated from deep in the crust during major crater formation are distributed as ejecta (Collins *et al.* 2005; Osinski *et al.* 2011, 2012), blanketing the pre-existing strata. 'Impact winter' describes a scenario in which the sheer volume of dust in the atmosphere blocks sunlight and causes drastic cooling of land surfaces (Covey *et al.* 1994). This means that among other, longer-term effects (see Walkden & Parker 2008) we note that the potential to change the mineralogy available to the atmosphere exists after the dust has settled, until weathering and removal returns the surface veneer to the normal clay-rich state.

On Earth, Kfs is spatially heterogeneous owing to a range of tectonic, magmatic and land surface processes that control the distribution of typical upper crustal rock types (Pankhurst 2017; see Fig. 1). Underneath Earth's surface veneer, Kfs and the textures it forms are heterogeneously distributed (as are all minerals). Some rock types such as basalt and limestone contain <<1% Kfs, whereas some granitoids can exceed 60%. Via the excavation of local-scale rocks from the Earth's crust and redistribution across a global-scale surface, major meteorite impact events hold the potential to change the Kfs content of dust available to the atmosphere in a geological instant. Has this ever occurred, and are there strikes that produced similar amounts of dust, but without Kfs?

Constructing a database of dust-refreshing events

Our aim is to collate the available data concerning scale and Kfs content of ejecta from meteorite impact events in a manner that allows first-order comparisons to be made. We begin with the most complete resource available, the Earth Impact Database (PASSC 2017), and later discuss inherent limitations to this approach. The largest crater diameter according to the Earth Impact Database is 160 km (Vredefort). All the confirmed bolide impacts with collapsed crater diameter >16 km were collated and for the purposes of this work are considered 'major' as they represent the top order of magnitude of crater diameters (D). From these major strikes a subset from 600 to 0 Ma was selected ($n=43$), to which we added the Alamo impact event ($D=65$ km; Pinto & Warmer 2007). We restricted our time window to exclude times >600 Ma because the post-600 Ma geological record is more complete, tectonic reconstructions are more accurate, it is the period of Earth history in which soil formation and vegetative cover predominate, and this interval afforded us a dataset of useful size. These 44 impacts were assessed for (1) their target rocks' KFF, and (2) the volume of the ejecta blanket resulting from the impactor. For craters with age determinations better than ±20 myr ($n=35$), we were able to determine (3) their palaeogeographical location at the time of impact, which, when combined with (4) the lateral spread, thickness and particle sizes of the ejecta blanket, allowed us to estimate (5) the post-strike KFF of the global average land surface. We chose a cut-off of ±20 myr to limit the uncertainty produced by tectonic reconstructions and still retain c. 75% of the database.

Assessment of Kfs abundance in meteorite impact event target rocks and average global surface veneer

The level of detail available concerning mineralogy of target rocks in the literature is highly variable. Kfs abundance, if not directly measured, was determined from target rock descriptions. A robust

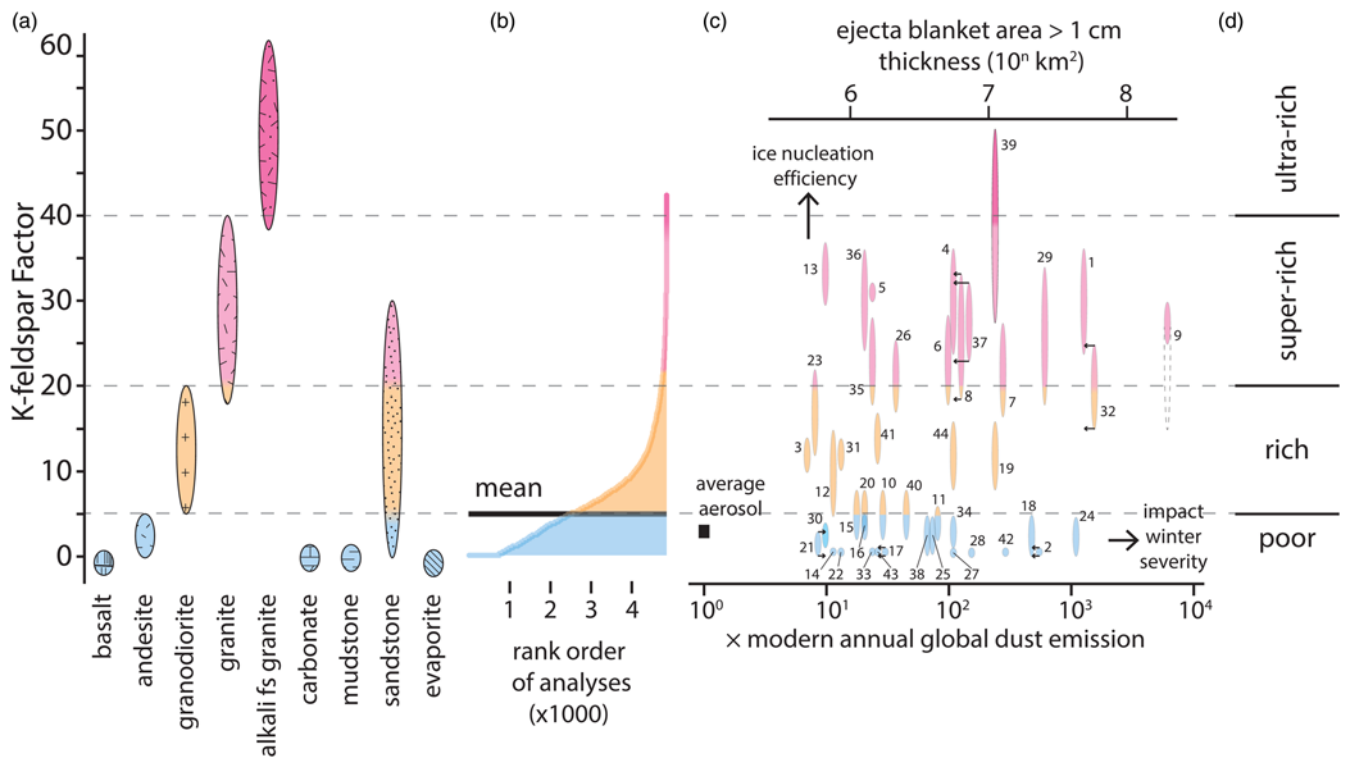


Fig. 1. Meteorite impact events change Kfs availability to the atmosphere. Major meteorite impact events since 600 Ma have produced ejecta blankets ranging in both total volume and KFF by factors of >100 and >50 respectively. **(a)** KFF of the most important upper crustal rock types. **(b)** Average KFF in soil from across the USA (Smith *et al.* 2014) is used as a proxy for the Earth's background surface veneer. **(c)** KFF of impact crater target rocks plotted against volume of <200 µm size fraction ejected and expressed as a function of modern dust emission, and ejecta blanket area (includes continents and oceans); labels as for Tables 1 and 2. Arrows denote the potential magnitude of direct (impact winter) and indirect (ice nucleation) effects on climate. **(d)** Qualitative KFF divisions are based on: poor, <average soil; rich, >average soil; super-rich, >highest average upper continental crustal estimate (Taylor & McLennan 1995); ultra-rich, approaches or exceeds modern atmospheric aerosol per cent and soil by a factor of 10.

assessment of Kfs abundance can even be made from field descriptions. This is because Kfs is (1) absent or negligible in many major rock types (e.g. basalt, limestone), and (2) a diagnostic rock-forming mineral used in quantitative terms within the nomenclature of granitoid suites (e.g. granitic or granodioritic; high and low Kfs respectively; see Streckeisen 1974). Where available, whole-rock geochemical data from granitoids (or metamorphic equivalents) were used to generate CIPW norms.

Terrigenous sediments are composed of between 5 and 15% feldspar, of which Kfs has been regarded as the most common owing to its higher availability and stability than plagioclases (Pl) under normal surface conditions (Folk 1980). The largest single continent-scale dataset of soil mineralogy gathered to date (Smith *et al.* 2014), however, returns an average Kfs:Pl of 1:1.7. Authigenic Kfs is common in marine sediments, but only in rare cases do abundances exceed 2% (Buyce & Friedman 1975). We assumed a low total Kfs content in sedimentary target rocks where mineralogical data were not available, as high Kfs content is reported only from immature sediments derived from granites or felsic large igneous provinces (e.g. Eriksson *et al.* 1994). Furthermore, the sandstone packages reviewed here are often intercalated with clay- and carbonate-dominated rock types, which dilute Kfs content in the overall sequence.

The most complete overview of meteorite impact event target rocks to date (Osinski *et al.* 2007) demonstrates that target geology ranges from highly homogeneous to heterogeneous. Volumes of individual rock types, and by extension the Kfs content, can be estimated with accuracy if outcrop maps (e.g. Lambert 2010) and/or subsurface observations, such as from geophysical surveys and drillcores (e.g. Tsikalas *et al.* 1998; Bron & Gostin 2012) are available. The corollary is that poor exposure and limited subsurface information leads to a broader range of plausible Kfs content.

A summarized description of target rocks and minerals from each crater is accompanied by an assessment of KFF in Table 1. Because the level of detailed lithological description available in the literature is variable and cannot be presented with equal confidence, the abundances are reported as a range of plausible values rather than a value with an uncertainty. Descriptions characterized by complex, heterogeneous lithologies, but without well-understood proportions, resulted in a larger range of plausible KFF. Lithology of target rocks can be matched to their ejecta blankets where they are sufficiently preserved (Gostin *et al.* 1986; Horton & Izett 2005; Thackrey *et al.* 2009), which validates this approach.

A global average KFF of five is derived from the most exhaustive database of soil mineralogy published to date (Smith *et al.* 2014). These soil data are used as the best available mineralogical surface veneer dataset for an entire, continental-sized landmass with a long and mixed geological history; as such they are the most representative available. A global atmospheric aerosol KFF of three (derived from Atkinson *et al.* 2013) is consistent with this value, given Kfs is present mainly in the silt, rather than clay size fraction (Claquin *et al.* 1999), and is more likely to be under-represented in aerosolized soil.

Ejecta blanket calculations

The scale of ejecta blankets is fundamentally linked to the volume of the transient cavity formed during the first stages of impact cratering, which is difficult to calculate with certainty. All the impacts considered here formed complex craters (including collapse of the transient cavity inwards), and have undergone variable modification and erosion post-impact. Owing to the considerable sources of uncertainty in any single case (see section below) and to maintain equal treatment, in the first instance we used the measured

Table 1. Assessment of KFF in target rocks from meteorite impact events

Number	Crater	KFF	Notes	Reference(s)
1	Acraman	24–36	Target rocks are dacites, rhyolites and A-type granites, which are dominated by K-feldspar (Williams 1986; Pankhurst <i>et al.</i> 2011b). These lithologies form the ejecta horizon (Williams 1986)	Williams 1986; Pankhurst <i>et al.</i> 2011b
2	Alamo	0–1	Thick Paleozoic carbonate sequences in a marine basin (Pinto & Warme 2007). Age taken as the middle of the Frasnian (Morrow <i>et al.</i> 2009)	Pinto & Warme 2007; Morrow <i>et al.</i> 2009
3	Ames	10–14	c. 700 m of carbonate, underlain by granite basement; 11% Kfs	Carpenter & Carlson 1992
4	Araguainha	24–36	Araguainha Granite (30–40% Kfs; Machado <i>et al.</i> 2009) and some metapelitic. Overlain by >1 km of Paleozoic cover (Tohver <i>et al.</i> 2012; Silva <i>et al.</i> 2016)	Machado <i>et al.</i> 2009; Tohver <i>et al.</i> 2012; Silva <i>et al.</i> 2016
5	Boltyshev	30–32	Porphyroblastic granites (age c. 1.55 Ga) and biotite gneisses; the average of 40 of these basement rocks (Gurov <i>et al.</i> 2006) produces a normative orthoclase component of 31%	Gurov <i>et al.</i> 2006
6	Carswell	18–28	A variety of basement rocks (granitoids; quartz–feldspar and pelitic gneisses; iron formation and metagabbro) are intruded by abundant granite pegmatite (in places up to 60%), which itself is 40–60% Kfs (Harper 1981). It is unclear how thick the overlying sandstones of the Athabasca Basin were at the time of impact	Harper 1981
7	Charlevoix	17–27	Charnockite gneiss, granite gneiss, migmatized paragneiss, and some anorthite (Trepmann <i>et al.</i> 2005). Kfs shock features within 2 km of impact structure centre (Robertson 1975)	Robertson 1975; Trepmann <i>et al.</i> 2005
8	Chesapeake Bay	19–33	Hit the Langley Granite, which is >20% microcline (Horton <i>et al.</i> 2005). Wet, unconsolidated sediments or sedimentary rocks were present on top (Horton <i>et al.</i> 2007, 2009), which may reduce the % Kfs in the excavation. However, detailed work on the ejecta shows the feldspar is all Kfs (Horton & Izett 2005)	Horton <i>et al.</i> 2005, 2007, 2009; Horton & Izett 2005
9	Chicxulub	15–30	Cratering affected entire crust, and thus it is possible that a range of lithologies should be present. This could conceivably result in a convergence of Kfs from upper continental crustal values toward normative bulk crust (20.1% and 6.5% orthoclase respectively; Taylor & McLennan 1995). The pre-impact target has been defined as c. 3 km of sedimentary cover (Ward <i>et al.</i> 1995) over crystalline basement (Morgan <i>et al.</i> 2016). The cover sequences are dominated by carbonate rocks (e.g. Ward <i>et al.</i> 1995; Stinnesbeck <i>et al.</i> 2004). Drilling past this cover has recovered predominantly a coarse-grained, roughly equigranular granitic rock that is locally aplitic or pegmatitic and, in a few cases, syenitic (Morgan <i>et al.</i> 2016). On the basis of these data we estimate a c. 25–30% Kfs abundance, yet caution that the presence of common lower crustal rocks, such as gabbros (no Kfs), may impart a diluting of these values, which is indicated in Figure 1	Ward <i>et al.</i> 1995; Stinnesbeck <i>et al.</i> 2004; Morgan <i>et al.</i> 2016
10	Clearwater East	2.5–7.5	Amphibolite- to granulite-facies metamorphosed tonalites, granodiorites, quartz monzonites, amphibolites. Essentially the same as Clearwater West but no Ordovician limestone (Schmieder <i>et al.</i> 2015)	Schmieder <i>et al.</i> 2015
11	Clearwater West	1.5–6.5	Basement is Proterozoic gneiss, granite, containing Kfs and plagioclase, underlying limestone (Simonds <i>et al.</i> 1978)	Simonds <i>et al.</i> 1978
12	Dellen	5–15	Gneissic granodiorite (Svensson 1968); at most the orthoclase content is 15% according to the definition of granodiorite	Svensson 1968
13	El'gygytgyn	27–37	Siliceous volcanic rocks are the exclusive target (Melles <i>et al.</i> 2011), which contain abundant Kfs, and the CIPW norm of the average target rock composition (Gurov & Koeberl 2004) is 28.4% by volume. Ejecta are noted to contain a high proportion of glass (Pittarello & Koeberl 2013b), which represents an important example for further study, and could refine this range of plausible Kfs values downwards significantly	Gurov & Koeberl 2004; Melles <i>et al.</i> 2011; Pittarello & Koeberl 2013b
14	Glikson	0–1	Sedimentary basin; quartzose sandstone (Macdonald <i>et al.</i> 2005)	Macdonald <i>et al.</i> 2005
15	Gosses Bluff	2.5–7.5	Sedimentary. The conglomerate and sandstone could contain Kfs, but none is noted (Glikson 1969)	Glikson 1969
16	Haughton	3–5	Mainly carbonates (top 1700 m); however, the basement is gneiss. Some (rare) granitic clasts noted. Whole-rock data show impactite contains only 2.9% Al ₂ O ₃ , which implies a very low feldspar content (Robertson & Sweeney 1983). There is some debate regarding the dating of this structure (39 Ma, Sherlock <i>et al.</i> 2005; 23.5 Ma, Young <i>et al.</i> 2013); we elected to use the more recently published age in Table 2	Robertson & Sweeney 1983; Sherlock <i>et al.</i> 2005; Young <i>et al.</i> 2013
17	Kamensk	0–1	Marls, sandstone, chalk (Izett <i>et al.</i> 1994)	Izett <i>et al.</i> 1994

(continued)

Table 1. (Continued)

Number	Crater	KFF	Notes	Reference(s)
18	Kara	3–15	c. 5.5 km of mainly Paleozoic sedimentary rocks with minor diabase dikes and sills (Koeberl <i>et al.</i> 1990), derived from and overlying mainly upper Proterozoic schists, metamorphosed rhyolite and tuff (which do not crop out but are intersected in drillcore; Mashchak 1991), along with shales, porphyries and sandstones (Trieloff <i>et al.</i> 1998). Some impactites are reported as containing abundant quartz, feldspar and minor zircon (Trieloff <i>et al.</i> 1998), which is consistent with both metamorphosed rhyolitic or porphyry lithologies and sediments derived from them	Koeberl <i>et al.</i> 1990; Mashchak 1991; Trieloff <i>et al.</i> 1998
19	Kara-Kul	8–16	Slightly metamorphosed sedimentary rocks of Paleozoic age, intensively folded and intruded with granites (Gurov <i>et al.</i> 1993; Osinski <i>et al.</i> 2007). Age generally considered to be <5 Ma (Napier 2006; Kelley 2007), with an upper limit of 30 Ma (Yabushita 2002). This represents an uncertainty of +25 myr from the generally accepted age, yet its total range is <40 myr	Gurov <i>et al.</i> 1993; Yabushita 2002; Napier 2006; Kelley 2007; Osinski <i>et al.</i> 2007
20	Lappajärvi	2.5–7.5	Target rocks dominated by mica schist (Kfs-poor), although pegmatitic granite intrudes this mica schist over ‘large areas’ (Reimold 1982). Outcrop is poor inside the crater, but if the distribution of schist:granite is similar to that outside, where outcrop is much better, the granites occupy c. 10% by area, and where drilled, only mica schist is intersected (Pipping & Lehtinen 1992)	Reimold 1982; Pipping & Lehtinen 1992
21	Lawn Hill	0–3	Quartz-rich sandstones, silts and shales, overlain by Cambrian water-saturated dolomite (Salisbury <i>et al.</i> 2008)	Salisbury <i>et al.</i> 2008; Darlington <i>et al.</i> 2016
22	Logancha	0–1	Basalts and low-Kfs sediments (Feldman <i>et al.</i> 1983)	Feldman <i>et al.</i> 1983
23	Luizi	12–22	Arkosic sandstone, in which perthitic Afs is present (Ferrière <i>et al.</i> 2011)	Ferrière <i>et al.</i> 2011
24	Manicouagan	1–5	Garnet anorthosite and grey gneiss target rocks have no reported Kfs; however, some granitic or charnockitic rocks are present. Sanidine occurs in impact melt as overgrowths and is not present in original clasts (Floran <i>et al.</i> 1978). Mixing the 7–8 target lithologies to produce the chemistry of the impact melt can be summarized as 4.5% anorthosite, 55.5% mafic gneiss and 40% tan gneiss (with granitic–granodioritic composition) (Grieve & Floran 1978). Thus the tan gneiss would need to contain >12.5% Kfs for the dust to contain >5% Kfs. Because the least amount of quartz possible in a granite or granodiorite is 20%, and at this value the boundary between granite and granodiorite contains 65% plagioclase, this leaves a maximum of 15% distributed across Kfs and sodic feldspar within the tan gneiss. Tan gneiss samples rarely display $K_2O > Na_2O$ wt%, and thus the abundance of Kfs is probably <5%. Furthermore, the presence of <200 m Ordovician carbonates and shales (Spray <i>et al.</i> 2010) further indicates that KFF can be considered low in the ejecta blanket	Floran <i>et al.</i> 1978; Grieve & Floran 1978; Grieve & Head 1983; Spray <i>et al.</i> 2010
25	Manson	0–5	2.5 km of quartz–mud sedimentary rocks overlying a wide variety of crystalline rocks: gabbros, diabases, mafic volcanic rocks, leucogranites, graphic granites, oligoclase–biotite, biotite-amphibolite and amphibolite gneisses (Reagan <i>et al.</i> 1996). Intriguingly, K-feldspar is the most dominant mineral (in normative modes) of one of the impactites, probably owing to difference in comminution (Reagan <i>et al.</i> 1996). Given the abundance of quartz clasts (Reagan <i>et al.</i> 1996) and normal scarcity of authigenic Kfs in carbonate sediments (Buyce & Friedman 1975), this implies that the Kfs is present owing to preferential melting of the hydrated clay component of the sediments, which crystallized Kfs on cooling	Reagan <i>et al.</i> 1996
26	Mistastin	18–26	Crater is dominated by adamellite, with mangerite and anorthosite centrally (Marchand & Crocket 1977)	Marchand & Crocket 1977
27	Mjølnir	0–1	Several kilometres thick marine sediment succession of siliciclastic rocks, carbonates and evaporites (Tsikalas <i>et al.</i> 1998)	Tsikalas <i>et al.</i> 1998
28	Montagnais	0–1	The basement is relatively uniform in lithological composition and consists primarily of light green, fine- to medium-grained, chloritic metasubgreywackes and phyllites. Albite is the feldspar detected within the poorly sorted metasubgreywackes (Jansa <i>et al.</i> 1989)	Jansa <i>et al.</i> 1989
29	Morokweng	18–34	Metasedimentary rocks covering a granitoid + gabbro basement. Planar deformation features observed in Kfs (Koeberl <i>et al.</i> 1997). Drillholes intersect high proportion of granophyre (Reimold <i>et al.</i> 2002)	Koeberl <i>et al.</i> 1997; Reimold <i>et al.</i> 2002
30	Oasis	1–4	Sandstone, siltstones, claystones (Martin 1969; Reimold & Koeberl 2014). Unclear as to Kfs content, yet most ‘Nubian Sandstones’ are quartz arenite (Wood 2013)	Martin 1969; Wood 2013; Reimold & Koeberl 2014
31	Obolon'	10–14	Gneiss and granites; whole-rock data from these (Gurov <i>et al.</i> 2009) give CIPW norms of c. 13 vol% Kfs	Gurov <i>et al.</i> 2009
32	Popigai	24–36	Target rocks are dominantly Precambrian biotite–garnet gneisses and granites, overlain by 1–1.5 km of sedimentary and metasedimentary rocks (Masaitis 2003). Bottomley <i>et al.</i> (1997) described 1.25 km of sandstones and carbonates overlying Precambrian, generally granitic, gneisses. Crystalline rocks in the southern part of the structure are often granitic (Kettrup <i>et al.</i> 2003). These crystalline lithologies are slightly elevated in Kfs with respect to regional basement, which is broadly andesitic to dacitic (Rozen 1990)	Bottomley <i>et al.</i> 1997; Kettrup <i>et al.</i> 2003; Masaitis 2003
33	Presqu'ile	0–1	Greenstone belt (plagioclase-bearing basalts variably schistose) with tonalite intrusions (Higgins & Tait 1990)	Higgins & Tait 1990

(continued)

Table 1. (Continued)

Number	Crater	KFF	Notes	Reference(s)
34	Puchezh-Katunki	10–14	2 km of terrigenous or carbonate sedimentary rocks overlying gneisses and amphibolites (Masaitis & Mashchak 1990). The gneisses are plagioclase and hornblende dominated, and are variably granitized (Fel'dman <i>et al.</i> 1985)	Fel'dman <i>et al.</i> 1985; Masaitis & Mashchak 1990
35	Ries	24–36	Sandstones and carbonate (600–700 m) overlying mostly feldspar-rich granite (Stöffler <i>et al.</i> 2001). Crystalline basement is calculated as contributing 35% to ejecta (Hörz 1982). Sanidine is observed as the most abundant matrix mineral in melt (Osinski 2004)	Hörz 1982; Stöffler <i>et al.</i> 2001; Osinski 2004
36	Rochechouart	30–32	Metamorphosed plutonic and sub-volcanic rocks (Kraut & French 1971) mapped in detail by Lambert (2010). Characterized by granites and gneisses after granitoids, which vary in Kfs content in decreasing order from leptynites (gneissic alkali granites), to granites and to paragneiss (plagioclase dominant feldspar). The target area is composed of paragneiss c. 60%, leptynite c. 20%, granite c. 20%	Kraut & French 1971; Lambert 2010
37	Saint Martin	18–28	Basement of Proterozoic granite gneisses of varying (but often high, 30–40%) Kfs. Melt CIPW norms have Kfs >25% (Reimold <i>et al.</i> 1990)	Reimold <i>et al.</i> 1990
38	Saqqar	17–27	Siliciclastic rocks. Include feldspar in some units but minor in overall sequence. Alkali feldspar grains directly observed but no chemical information is available (Kenkmann <i>et al.</i> 2015)	Kenkmann <i>et al.</i> 2015
39	Siljan	19–33	Granite and minor diabase sills and dikes (Komor & Valley 1990). Detailed descriptions include adamellite and aplitic granites. Both Siljan and Dala granites are high-K (>4.9 wt% K ₂ O). Where directly measured, K-feldspar modes are between 28 and 52% (Lehnert <i>et al.</i> 2012)	Komor & Valley 1990; Lehnert <i>et al.</i> 2012
40	Slate Islands	15–30	Mixed crystalline crust including felsic porphyries interlayered with varying sedimentary and volcanic sequences (Sharpton <i>et al.</i> 1996)	Sharpton <i>et al.</i> 1996
41	Steen River	2.5–7.5	1.4 km of carbonates, evaporites and shales, overlying Precambrian granitic gneiss (Grieve <i>et al.</i> 1998). Some granite basement intersections are super rich in Kfs, yet the lithoclasts in the brecciated unit are mostly granodiorite (Molak 2001)	Grieve <i>et al.</i> 1998; Molak 2001
42	Tookoonooka	1.5–6.5	Hit marine basin; impact horizon of quartz, clay, mudstones (Bron & Gostin 2012)	Bron & Gostin 2012
43	Tunnunik	5–15	Carbonate rocks (Late Devonian alteration prior to impact means oldest age should be c. 360 not c. 450 Ma) (Kenkmann <i>et al.</i> 2015)	Kenkmann <i>et al.</i> 2015
44	Woodleigh	27–37	Mixed Proterozoic basement; contains granite but unclear how much Kfs is in gneisses (Hough <i>et al.</i> 2003)	Hough <i>et al.</i> 2003

Subset is since 600 Ma and within the top order of magnitude of crater diameter (*D*). Numbers correspond to those in Figure 1 and Table 2.

Table 2. Kfs availability in Earth's surface veneer as a result of meteorite impact events since 600 Ma

Number	Crater name	Age (Ma) ¹	±Ma	Plausible range in KFF of ejecta blanket		Crater diameter (D) (km)	Diameter of transient cavity (D_{tc}) (km) ²	Ejecta blanket volume (km ³) ³	× Modern dust a ⁻¹ ⁴ (2 Pg a ⁻¹)	% Area of primary continental deposition ⁵				Global KFF post-strike ⁶
				Upper	Lower					>1 cm	>1 mm	>100 µm	>10 µm	
1	Acraman	580	7	36	24	90	51	9209	1266	7.0	18	52	97	29.3
2	Alamo	382.1	0.5	1	0	65	37	3469	477	1.6	7	25	76	1.6
3	Ames	470	30	14	10	16	9	52	7					
4	Araguainha	254.7	2.5	36	24	40	23	808	111	0.7	3	14	47	16.7
5	Boltysh	65.17	0.64	32	30	24	14	175	24	0.2	1	3	13	8.3
6	Carswell	115	10	28	18	39	22	749	103	0.6	3	11	29	10.3
7	Charlevoix	342	15	27	17	54	31	1989	273	1.5	6	31	78	18.3
8	Chesapeake Bay	35.5	0.3	33	19	40	23	808	111	0.4	2	8	27	10.7
9	Chicxulub	64.98	0.05	30	15	150	85	42633	5862	7.8	33	94	99	27.3
10	Clearwater East	465	5	7.5	2.5	26	15	222	31	0.2	1	5	15	5.0
11	Clearwater West	290	20	6.5	1.5	36	20	589	81	0.5	2	11	39	4.6
12	Dellen	89	2.7	15	5	19	11	87	12	0.1	0	2	8	5.4
13	El'gygytgyn	3.5	0.5	37	27	18	10	74	10	0.1	0	1	4	6.0
14	Glikson	508	8	1	0	19	11	87	12					
15	Gosses Bluff	142.5	0.8	7.5	2.5	22	12	135	18	0.1	1	3	10	5.0
16	Haughton	23.5	2.0	5	3	23	13	154	21	0.1	0	2	10	4.9
17	Kamensk	49	0.2	1	0	25	14	197	27	0.2	1	3	14	4.4
18	Kara	70.3	2.2	5	0	65	37	3469	477	2.2	9	34	73	3.2
19	Kara-Kul	5	7	16	8	52	29	1776	244	1.0	5	20	59	9.1
20	Lappajärvi	76.2	0.29	7.5	2.5	23	13	154	21	0.1	1	3	13	5.0
21	Lawn Hill	472	8	3	0	18	10	74	10	0.1	0.4	1.5	4.0	4.9
22	Logancha	40	20	1	0	20	11	101	14	0.1	0	2	9	4.6
23	Luizi	573	8	22	12	17	10	62	9					
24	Manicouagan	214	1.0	5	1	85	48	7758	1067	5.0	22	60	100	3.0
25	Manson	73.8	0.3	5	0	35	20	542	74	0.4	2	9	20	4.5
26	Mistastin	36.4	4.0	26	18	28	16	277	38	0.2	1	4	14	7.4
27	Mjølnir	142	2.6	1	0	40	23	808	111	0.6	3	14	44	3.0
28	Montagnais	50.5	0.76	1	0	45	26	1151	158	0.5	2	10	43	3.1
29	Morokweng	145	0.8	34	18	70	40	4333	596	2.6	11	38	79	21.6
30	Oasis	120	8	4	1	18	10	74	10					
31	Obolon'	169	7	14	10	20	11	101	14	0.1	0	2	8	5.5
32	Popigai	35.7	0.2	25	15	90	51	9209	1266	4.4	19	53	98	21.7
33	Presqu'ile	500	8	1	0	24	14	175	24					
34	Puchezh-Katunki	167	3	5	1	40	23	808	111	0.7	3	13	42	4.2
35	Ries	15.1	0.1	28	18	24	14	175	24	0.1	0	3	11	7.0
36	Rochechouart	201	2.0	36	24	23	13	154	21	0.2	1	3	14	8.6
37	Saint Martin	220	32	32	28	40	23	808	111					
38	Saqqar	240	170	5	0	34	19	496	68					
39	Siljan	376.8	1.7	50	28	52	29	1776	244	1.5	6	21	67	27.8
40	Slate Islands	650	150	8	2	30	17	341	47					
41	Steen River	91	7	17	11	25	14	197	27	0.2	1	3	8	5.7
42	Toookoonooka	128	5	1	0	55	31	2102	289	1.5	6	15	36	3.4

(continued)

Table 2. (Continued)

Number	Crater name	Age (Ma) ¹	\pm Ma	Plausible range in KFF of ejecta blanket		Crater diameter (D) (km)	Diameter of transient cavity (D_{tc}) (km) ²	Ejecta blanket volume (km ³)	\times Modern dust a^{-1} ⁴ (2 Pg a ⁻¹)	% Area of primary continental deposition ⁵			Global KFF post-strike ⁶
				Upper	Lower					>1 cm	>1 mm	>100 μ m	
43	Tannanik	290	160	1	0	25	14	197	27				
44	Woodleigh	364	8	16	8	40	23	808	111	0.6	2	12	38
										76			

¹Ages used are from post-2009 references in Table 1, or otherwise collated from Jourdan *et al.* (2009) and by consulting the Earth Impact Database (PASSC 2017).

²Using a D_{tc}/D value of 1:1.75 (rounded to nearest kilometre).

³Calculated as half the transient cavity volume.

⁴Volume of size fraction $>200 \mu\text{m}$, calculated as 10% of ejecta blanket volume and using an average rock density of 2.75 g cm^{-3} .

⁵Ejecta blanket is mostly discontinuous; values are averages of thickness at those radii (Collins *et al.* 2005).

⁶Using the KFF of target rocks, $>10 \mu\text{m}$ isopach area, and assuming the rest of the continental area at that time had present-day global average KFF of five. Error bars are shown in Figure 3, and are calculated using the maximum and minimum values in the KFF of target rocks. Because the same equations to calculate the scale of areal extent (Collins *et al.* 2005) were used throughout, the associated errors are applied equally. This error is potentially large and non-linear, yet is not quantified, and so is not considered here. Potential errors in tectonic-plate reconstruction models, which could change the per cent of continental area under the ejecta blanket, are not quantified. Comparison of three models (Gurnis *et al.* 2012; Torsvik *et al.* 2012; Matthews *et al.* 2016), however, finds good agreement (e.g. supplementary material Fig. S1), and is likely to contribute substantially less uncertainty than that associated with primary deposition area, and continental subaerial v. subaqueous distribution.

⁷Special cases: the Acraman ejecta layer is stratigraphically well-defined as a marker horizon within the Bunyeroo Formation, which has a duration of 35 myr. The upper age limit of the Kara-Kul crater is 30 Ma, which is 25 myr from the generally accepted age of 5 Ma, yet the total uncertainty is <35 myr.

⁸Denotes the maximum age, with no minimum reported. Calculated for those craters in Table 1 with age determinations >20 myr.

crater value of D to approximate the diameter of the transient cavity (D_{tc}) by a fixed ratio of 1:1.75. This value is based on detailed analysis of evidence from Chicxulub (Morgan *et al.* 2002), which, as its target rocks were sedimentary cover over crystalline basement, is both the most studied and most typical geological scenario in our database.

Equations within the Earth Impacts Effects program <http://impact.ese.ic.ac.uk/ImpactEffects/> (Collins *et al.* 2005) were used to calculate the diameter and depth of the transient cavity (following terminology of French 1998), and ejecta thickness with distance for the subset of craters where appropriate (see palaeogeographical reconstructions and area calculations below). To check if our use of a fixed ratio caused significant differences in model outputs for each impact, parameters were fixed with geological evidence where available (e.g. target rock type and thus density and presence of water). In all instances where the following parameters are not available, an impact trajectory of 45° (statistically most likely), bolide density of 3000 kg m^{-3} (dense rock) and pre-atmospheric entry velocity of 17 km s^{-1} were used. For a fair comparison between these events, we did not attempt to reconcile strewn fields or measured ejecta blanket thickness with our calculations, for these are subject to post-deposition modification, and such measurements are limited to a minority of these events.

The D_{tc} value given by consistent application of the 1:1.75 relationship taken from the largest case (Chicxulub, where $D = 150 \text{ km}$) is normally an underestimation of the D_{tc} given by the program. In the smallest cases (i.e. Ames, $D = 16 \text{ km}$) D_{tc} is underestimated by $<20\%$. For the purposes of comparing Kfs availability post-strike between events, larger errors at the smaller end of the range of crater sizes are more acceptable than the opposite. Transient cavity depth is especially important for craters exhibiting pre-strike strata with differing Kfs abundance with depth. For consistency, we maintain use of the D_{tc} from the ratio of 1:1.75 described above. Around one-third to a half of the fragmented material either does not escape or falls back into the crater (Collins *et al.* 2005; Osinski *et al.* 2012); up to two-thirds could escape. As such, ejecta are dominated by material from the excavated zone as opposed to the (deeper) displaced zone (Osinski *et al.* 2011), yet rocks across the cavity depth can be found in ejecta (Osinski *et al.* 2008, 2012). It remains poorly known how much material is actually ejected and this may vary considerably on a case-by-case basis (Melosh 1989; Osinski *et al.* 2011). In our calculations of ejecta volume we use one-half of the transient cavity volume, to again maintain an underestimated final result.

In examples where thick, low-KFF sedimentary cover overlies high-KFF basement, we assume material from only the top half of the transient cavity contributed to the ejecta, in the absence of mass-balance calculations from the impacted rocks themselves (e.g. Hörz 1982). This step prevents the gross overestimation of Kfs, which owing to the normal low background would be more erroneous than underestimating by a little. This step produces differences in Kfs availability only for craters with diameter at the smaller end of the range, and applies to $<20\%$ of the dataset. Furthermore, because smaller craters produce less ejecta and so inherently have a smaller capacity to change the KFF of the global surface veneer, no first-order bias is anticipated in the later comparisons.

Melting has the potential to reduce the amount of Kfs released to the ejecta blanket. The proportion of melt volume to ejecta volume increases with energy transfer, which is a function of impactor size and velocity (Cintala & Grieve 1998). Even for the largest strike considered here, however, this melt volume is $<10\%$ of the transient cavity volume, and does not change substantially if comet densities (much lower) and velocities (potentially much higher) are used. It is worth noting that the processes of melt generation and emplacement are more complicated than first thought (Osinski *et al.* 2011). For instance, the El'gygytgyn impact crater provides evidence that more

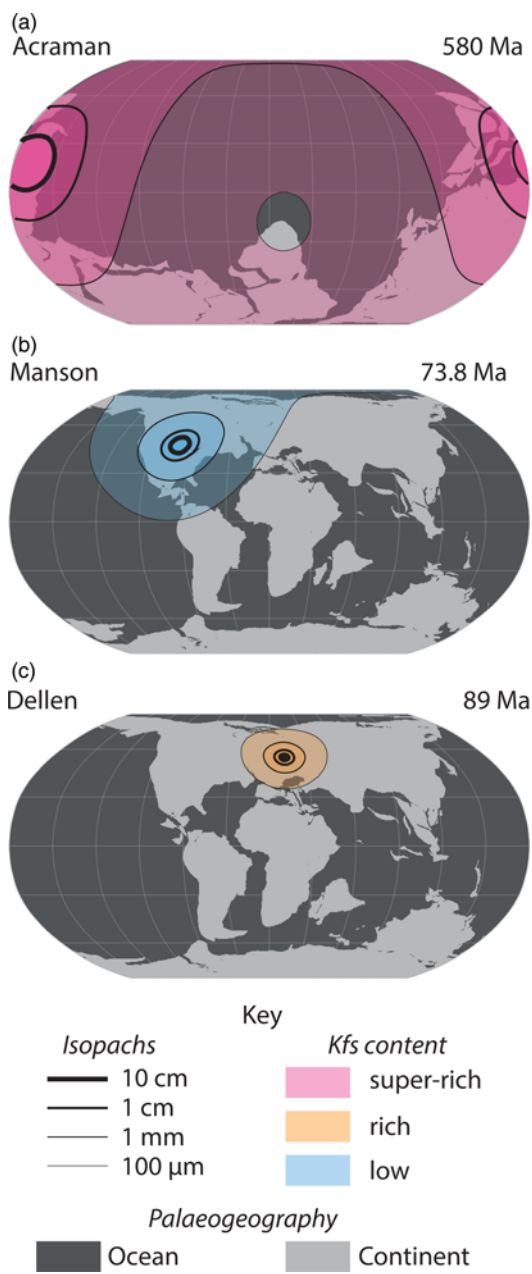


Fig. 2. Selected examples of Kfs abundance, primary distribution and palaeogeographical context of meteorite impact event ejecta. Isopachs are radial representations of an averaged thickness, which is expected to be regionally discontinuous (Collins *et al.* 2005). (See supplementary material Fig. S2 for all maps generated from those meteorite impact events with age uncertainties ± 20 myr, since 600 Ma.)

extensive melting can occur (Pittarello & Koeberl 2013a) and so illustrates the potential for uncertainty. Because average ejecta thickness with distance is more meaningful to global Kfs availability (see below) than the comparatively small difference that target rock melting of this scale would make to the ejecta blanket KFF, we do not include impact melt volume in our assessment.

Understanding of impact cratering is incomplete, and all individual model outputs should be considered highly uncertain. Nevertheless, the calculations of ejecta volume (see Table 2) are most sensitive to the transient cavity volume. Applying the same set of scaling laws (e.g. Croft 1984; Holsapple 1993, 2017; Collins *et al.* 2005) consistently across the largest 44 known impacts present in the rock record results in large relative differences in KFF and volume.

Dust volume calculations

Particles in the $<100\text{--}200\ \mu\text{m}$ range are mobilized by desert winds on ballistic trajectories close to the surface, and break apart or eject smaller particles on striking the soil (Mahowald *et al.* 2014). These smaller particles ($<c.\ 50\ \mu\text{m}$) are able to be entrained into the upper boundary layers, after which they can be transported long distances and enter the atmosphere (Mahowald *et al.* 2014). Hypervelocity impacts produce proportionally more fine material than surface or subterranean explosions (O'Keefe & Ahrens 1985). According to a regression based on scaled laboratory experiments, $c.\ 10\%$ of the fragmented ejecta would be $<200\ \mu\text{m}$ (O'Keefe & Ahrens 1985). If the volume of the ejecta blanket is 50% of the transient crater volume (as discussed above), it follows that the available volume of primary dust meaningful to the climate system immediately post-impact can be estimated as 5% of the transient cavity volume. This estimate of total dust production is presented for each impact event relative to modern dust emission as the lower horizontal axis in Figure 1c. This value of 5% is considered highly uncertain in any individual case, but does serve as the most reasonable estimate at present. The volume and flux of dust mobilized from the ejecta layer as part of normal aerosolization mechanisms is another flux that is difficult to estimate, which is why we consider the fraction of continental area to be useful (see below).

Palaeogeographical reconstruction and area calculations

Palaeogeographical context of a meteorite impact event has the potential to be as important as target rock KFF. For instance, if an ejecta blanket of size X composed of 20% Kfs spanned a large continental area (above sea level), the available Kfs across the surface of the Earth would be comparable with that caused by an ejecta blanket of size X with 40% Kfs that straddled a coastline. Approximately half the material (and Kfs) in this latter case would be deposited directly into the ocean and take no part in later aerosolization processes.

Palaeolatitude was estimated for the majority of meteorite impact events using the calculator of van Hinsbergen *et al.* (2015), and compared with both palaeolatitude and palaeolongitude estimated using geological maps and plate reconstruction models (Matthews *et al.* 2016, strikes <300 Ma; Scotese 2016, >300 Ma; see Fig. 2). This allowed both an estimate of ejecta blanket reach around the globe, and palaeogeographical context (ejecta coverage of continental v. ocean area) using GPlates (<https://www.gplates.org/>; Gurnis *et al.* 2012). Small circles were drawn in GPlates with radii corresponding to average ejecta thickness, derived from the same model as used to calculate the transient cavity volume (Collins *et al.* 2005).

To calculate the proportion of the Earth's continental area covered by ejecta blanket, 8-bit binary images (255: continents; 0: oceans) using an equal-area projection were exported from GPlates at high resolution (10 000 pixels width) and analysed for area using ImageJ (<https://imagej.nih.gov/ij/>; Rasband 2015). Images at the same pixel resolution were exported with coloured lines ($c.\ 3$ pixels wide, value between 0 and 255), to which a threshold was applied and deleted. This removal of the fine lines isolated regions of continent inside and outside the relevant circles (ejecta minimum thickness of 10 cm to 10 μm). The area of each region was measured, and used to calculate the area within each isopach. This value was then expressed as a proportion of the total continental area. Using this approach, a self-consistent prediction of global Kfs abundance immediately after a meteorite impact was derived.

Current limitations and future considerations

Database usage

The Earth Impact Database, at present, is not itself peer reviewed, but rather collates information from the 'hard' literature and seeks to

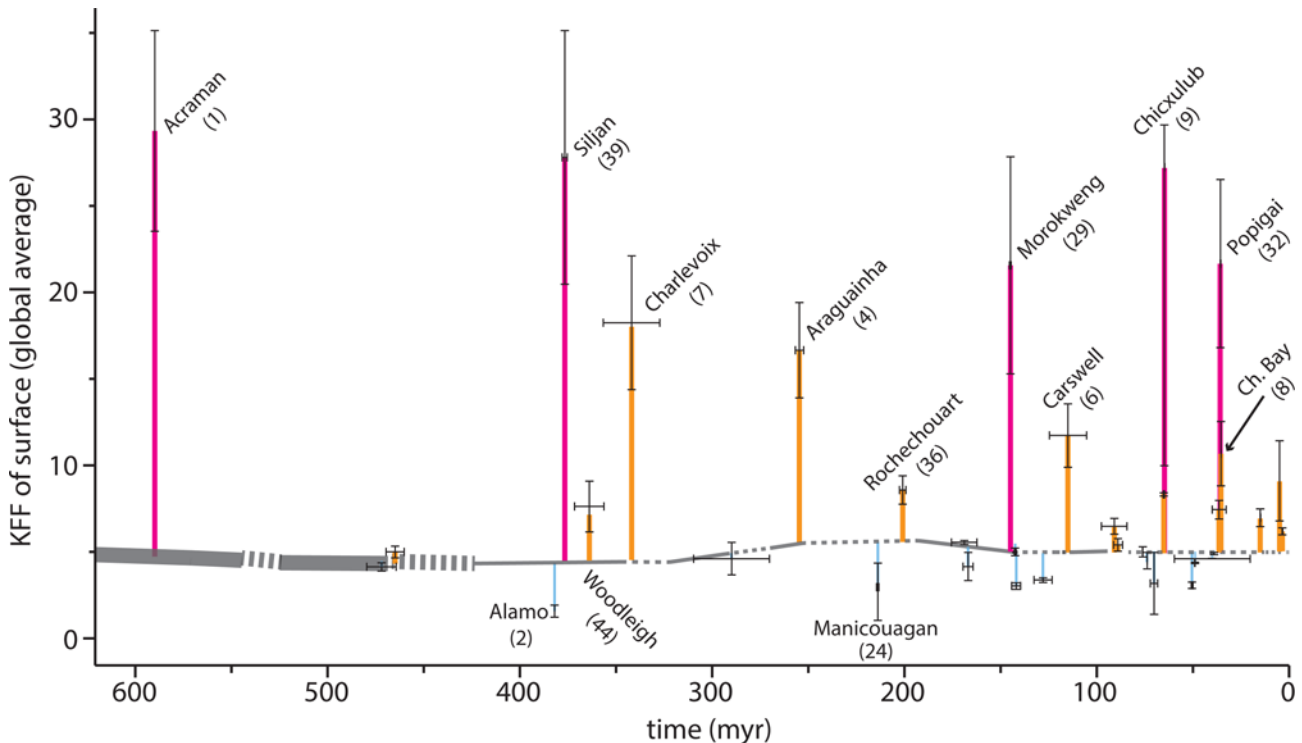


Fig. 3. Estimated global potassium feldspar factor in subaerial veneer since 600 Ma. All confirmed meteorite impact events with age uncertainty $\leq \pm 20$ myr and crater diameter > 16 km are represented. Error bars denote the upper and lower plausible range of KFF post-strike, which returned to background partly as a function of ejecta blanket volume. The modern baseline KFF is pinned to five (Pankhurst 2017), derived from a measured mean value of modern soil (Smith *et al.* 2014). Dashed background indicates approximate timing of glacial regime (reasoned to cause higher variability than non-glacial regime; see Pankhurst 2017). Of the well-dated subset that allow modelling, the 13 furthest departures from background are named. Numbers correspond to Tables 1 and 2.

present it in a consistent and accessible format. Debate concerning accuracy of some of the information listed is currently continuing. For instance, recent refinement to a few of the crater diameter data (Osinski & Ferrière 2016) suggests that improvements to our results can be expected in future studies. Nevertheless, for our purposes here (see section ‘Constructing a database of dust-refreshing events’) it is necessary to consider, and treat, a large number of impact events consistently.

Calculations

The primary amount and distribution of dust available to be remobilized after emplacement of an ejecta blanket calculated here are gross oversimplifications in each case. We supply the outputs attached with the following caveats.

The volumes calculated are internally consistent and are most sensitive to a parameter (transient cavity diameter) that has also been calculated and presented consistently (Earth Impact Database, PASSC 2017), yet these values include their own individual uncertainties that are not considered here.

The calculations of ejecta thickness with distance from a crater (Collins *et al.* 2005) were applied consistently and are helpful for visualizing and comparing the scale of events. However, the isopachs are not considered to be spatially precise, but rather approximate an average value of thickness at that distance (see Collins *et al.* 2005). These maps provide for an internally consistent method to assess continental v. oceanic distribution, which allows us to attach proportionately more relevance to regions closer to a crater than further away from it.

This relevance is calculated by using plate reconstruction models, which also include uncertainty we do not explicitly factor in. However, the comparison between independently derived palaeo-latitudes (Fig. S1) lends confidence that these models have

sufficiently small uncertainties for our purposes. Even when combined with the caveat attached to isopachs above, at the very least we can safely assume our approach introduces far more accuracy to our final global Kfs availability calculation than it removes.

We note that a portion of the continents as defined by GPlates polygons was subaqueous at each time considered. This portion is not estimated because of large differences in uncertainties across the 600 myr considered. The proportion of subaerial continental area covered by ejecta into continental interiors is likely to be underestimated slightly as a result, as shallow sea and shelf areas are typical of continental margins. This error is probably only a few per cent from small strikes and less for larger strikes. The possibility of simultaneous meteorite impact events (e.g. Spray *et al.* 1998), which would complicate these calculations, is low in comparison with the size of the dataset, and is not considered here.

The KFF of lithologies hosting the impact crater is considered a good guide to the KFF in the associated ejecta blanket, an assumption supported by studies that successfully link craters with their blankets using shared lithology and mineralogy (Hörz 1982; Gostin & Zbik 1999; Thackrey *et al.* 2009). However, determining an accurate abundance is difficult without detailed lithological maps, mineralogical notes and an assessment of melt percentage in distal ejecta. Presenting a range of plausible KFF values rather than a single value with an uncertainty is considered to better reflect this limitation.

Aerosolization of the ejecta blanket and return to background

Aerosolization potential (see Shao *et al.* 2011) after primary deposition is governed by landscape processes that are not within the scope of this work. What kind of primary spatial distribution is actually meaningful, and estimating the timescales of return to

background Kfs availability, could be highly sensitive to climatic conditions at the time of individual meteorite impact events. Therefore how an instantaneous, voluminous dust source is redistributed after its primary deposition compares with the present dust cycle is unknown, and difficult to estimate owing to numerous feedbacks (Shao *et al.* 2011).

The rock record

The meteorite impact event record is incomplete, although all craters still present (not subducted) on Earth >85 km in diameter are likely to have been recognized by now (Kenkemann *et al.* 2015). We note that there are examples of low, average and high KFF across the range of crater size. Because much smaller craters than 85 km are calculated to effect considerable changes to global KFF, this missing record must be taken into account by future efforts to compare this parameter against other data in the rock record. Finally, the record is more complete with decreasing age; any real relationship observed between surface veneer KFF and other data should become stronger through time to the present.

We include only meteorite impact events that are reported with an age determination of ±20 myr in our assessments. This threshold provides reasonable accuracy when linking time of event to tectonic context. Better age-dating of impact events will lead to both (1) more events being able to be considered for Kfs availability and (2) increased confidence in any interpretations arising.

The pre-strike distribution of Kfs across the Earth is also not considered in this study. The possibility remains that, for instance, high-Kfs dust generated by a meteorite impact event covered land surfaces containing zero Kfs or very high-Kfs dust, meaning the upsurge calculated is under- or overestimated for each scenario respectively. This potential source of uncertainty becomes important for small strikes generating extremely high or low Kfs dust.

Results: target rocks, scale of ejecta blankets and primary global distribution

KFFs typical of major lithologies (Fig. 1a), and those estimated in ejecta from the most relevant subset of Earth's cratering record (Fig. 1c; $n=44$) are presented alongside that of modern soil (Fig. 1b), which we use as the best available guide to the normal regime (see also Table 1). There is no systematic relationship between the scale of meteorite impact event and KFF of target lithology(ies) (Fig. 1c), which is unsurprising because of the randomized location of strikes and heterogeneous distribution of Kfs. Sixteen meteorite impact events mobilized low-KFF rocks. Half of the strikes mobilized Kfs to at least greater than the mean global surface value. Around a quarter contain Kfs that probably exceeded average upper continental crust (Taylor & McLennan 1995). Targets with mixed lithologies generally resulted in estimated KFF at or slightly higher than average surface availability.

During desert wind events, particles up to 100–200 µm are broken up into smaller fragments (<c. 50 µm) by saltation, before being entrained and carried long distances in the atmosphere (Mahowald *et al.* 2014). Because the proportion of ejecta fragments generated by a hypervelocity impact <200 µm can be estimated (c. 10 vol%; O'Keefe & Ahrens 1985), simple comparisons of Kfs availability to the atmosphere can be made between normal conditions and those after individual meteorite impact events.

Selected palaeogeographical reconstructions of ejecta distribution, a guide to dust generation, are presented in Figure 2 (all are provided in supplementary material Fig. S2). The assessment of ejecta distribution across continent v. ocean (Fig. 2 and Fig. S2) allows a quantitative estimate for the globally averaged surface veneer KFF to be calculated, and is plotted in Figure 3 as a timeline since 600 Ma and using KFF = 5 as a baseline (Pankhurst 2017).

Each post-strike value is simply the weighted average of the KFF of continental surface area inside the 10 µm isopach (the KFF of the target rocks), and outside it (KFF = 5). We assume the area within the 10 µm isopach represents a meaningful, and at least internally consistent, approximation of the surficial extent of particles that can be readily aerosolized shortly after primary deposition.

This is because, although smaller particles (ejected over a larger area) are more easily mobilized, the ejecta blanket's capacity to act as a continuing dust source increases towards the strike location (thicker blanket, yet smaller area). Our calculations, which are conservative at each step, show that many meteorite impact events generated a volume of particles <200 µm between two and three orders of magnitude greater than that of modern annual dust emission by mass (Table 2; also shown in Fig. 1), although in many instances a significant portion would probably be deposited directly in the oceans (Fig. 2 and supplementary material Fig. S2). Owing to the global scale of ejecta blankets, we gauge them to represent highly important instantaneous dust sources, whose persistence is discussed below.

Toward understanding alkali feldspars' role in the climate system

There are many areas for improvement in both accuracy and precision of our calculations of Kfs availability to the atmosphere. However, the review of target rocks shows that KFF ranges from zero to >60. The volumetric estimations of the dust portion of ejecta blankets often exceed that of modern annual dust emission (1–3 Pg; Astitha *et al.* 2012) by two to three orders of magnitude (Table 2). Improved assessment of crater diameter (Osinski & Ferrière 2016) leading to changes of c. 10–20 KFF do influence our results, although considerably so only at the higher end of the range.

For instance, using Osinski & Ferrière's (2016) data, ejecta volume from Manicouagan would be c. 50% larger, although it would have a minimal influence on globally averaged surface veneer KFF. Chicxulub ejecta volume would be closer to double, yet its influence already reaches around the globe and in this case the most important factor becomes the KFF of the target rocks. Therefore, and despite the caveats detailed above, our attempt at quantifying Kfs availability demonstrates that a considerable range in both absolute abundance and KFF existed in ejecta blankets.

Context for future studies

Kfs is common in the Earth's upper crust. It accounts for c. 20.1 wt % (Taylor & McLennan 1995). Kfs is the key constituent of many granitoid types (in particular, syenite, alkali feldspar granite and granite *sensu stricto*) and some extrusive equivalents, which are heterogeneously distributed through tectonic and magmatic processes (Pankhurst *et al.* 2011a, 2011b, 2013). The distribution of different rock types across the continents results in major differences in the KFF of dust sources at local scales (Scheuvens *et al.* 2013; Smith *et al.* 2014).

Arid areas contribute a disproportionate amount of both total dust (Marticorena 2014) and Kfs owing to the low soil surface stability and lower rates of chemical weathering respectively. KFF in dust has been measured between 0.18 and 25, which reflects local upwind dust sources (Kandler *et al.* 2009, 2011; Díaz-Hernández *et al.* 2011). On average, however, Kfs contributes c. 3 wt% to the global mineral aerosol budget, and becomes comparatively well mixed in the atmosphere (Atkinson *et al.* 2013). This means that the mineralogy of atmospheric dust reflects an averaged global surface veneer mineralogy.

Background Kfs availability to the atmosphere, at a global scale, is buffered at low levels owing to chemical weathering and heterogeneous distribution of both high- and low-Kfs rock types

(Pankhurst 2017). Instances of zero levels of atmospheric Kfs, such as prior to the first true granite formation and instance(s) of Snowball Earth, follow a logic that can be reasoned without any direct measurement (Pankhurst 2017). Placing upper limits on Kfs availability is more challenging to attempt with any useful degree of accuracy. However, we show here that global-scale dust-producing events can be quantified, and time-stamped, which implies that a way forward is possible.

For example, the emplacement of felsic large igneous provinces (Pankhurst *et al.* 2011a), particularly those typified by extensive, shallow-emplaced and highly evolved magmas, has the potential to cause at least regional spikes in Kfs availability (Pankhurst 2017). Glacial periods are linked to greater atmospheric dustiness (Fuhrer *et al.* 1999; Lambert *et al.* 2008; Valbelonga & Svensson 2014). Rapid ice-sheet retreat has the potential to increase the abundance and proportion of Kfs available to the atmosphere by exposing fresh, finely milled rock powder (Pankhurst 2017). Compared with the timescales of these terrestrial processes, however, meteorite impact events are instantaneous, and have the potential to effect more dramatic change in surface KFF by distributing local rocks over global scales.

Multidisciplinary study is needed

It is reasonable to hypothesize that global cloud behaviour, and by extension climate, is sensitive to Kfs availability. Attributing measurable changes to the scale of possible impacts on weather and climate this may have, however, is non-trivial (Storelvmo *et al.* 2011; Boucher *et al.* 2013; Yang *et al.* 2015; Tan *et al.* 2016; Storelvmo 2017). This is partly because globally averaged land surface KFF today is neither at a high nor a low with respect to the rest of Earth history (Pankhurst 2017). The rock record preserves an abundance of information that detailed multidisciplinary study can extract, and use to reconstruct palaeoclimate dynamics (e.g. Shields *et al.* 2003; Trela *et al.* 2018). It is possible that Kfs availability is important in palaeoclimate dynamics, yet recognition has not occurred, as the importance of Kfs to cloud nucleation was discovered only recently (Atkinson *et al.* 2013; Harrison *et al.* 2016; Whale *et al.* 2017). Comparatively well-dated examples of extreme availability of Kfs should be useful in testing hypotheses concerning any relationship between changes to atmospheric Kfs and climate.

Using bolide impacts to calculate time-stamped Kfs availability

Owing to atmospheric mixing, natural mineralogical variation in the atmosphere that allows effects to be linked and quantified is better captured by regional patterns within similar climatic conditions (Glaccum & Prospero 1980; Prospero *et al.* 1981; Jeong 2008; Atkinson *et al.* 2013). Yet this global mixing also raises an opportunity. Any sudden temporal changes to global surface mineralogy should be reflected in global aerosol mineralogy and represent a chance to gauge potential effects. The absolute age of a meteorite impact event need not be known precisely for these studies to be conducted. Strata above and below ejecta layers contain relative age information inherently linked to proxies of environmental conditions, which is more important than absolute age.

The scale of meteorite impact events is of equal importance to the KFF of target rocks when calculating global Kfs availability. For example, Manicouagan, Tookoonooka, Alamo and Kara are in the top 10 craters for size, yet cannot be said to have changed global Kfs availability considerably. Palaeo-continental context is also important (Fig. 2 and supplementary material Fig. S2). Despite Kara-Kul ($D = 52$) mobilizing $10 \times$ the ejecta volume of Rochechouart ($D = 23$ km), both are calculated to have raised surface veneer

KFF to 8–9. This is due to c. 40% of Kara-Kul's ejecta blanket being deposited across ocean, and Rochechouart containing c. $2\text{--}3 \times$ the KFF in its target rocks (see Fig. S2).

Granites appear to be the key

Understanding why Kfs ice nucleation is so efficient under mixed-phase cloud conditions has been advanced by identification of active ice nucleation sites (Zolles *et al.* 2015), *ab-initio* modelling (Pedevilla *et al.* 2016) and direct observation of ice formation on Kfs surfaces (Kiselev *et al.* 2017). Crystal topography related to phase separation has recently been linked to exceptional ice nucleating properties (Whale *et al.* 2017). This helps explain why samples of sanidine (high-temperature Kfs polymorph) in early experiments did not nucleate ice well, and potentially why some samples of albite (anti-perthite; the Ab is the host of Kfs lamellae) are excellent ice nucleators (Whale *et al.* 2017).

Sanidine is common in volcanic rocks with similar bulk chemistry to granites, often observed in explosive super-eruption deposits where they are quenched from magmatic temperatures (e.g. Christiansen 2001). Based on present evidence it appears that volcanic eruptions, although overcoming the clay barrier, are less likely to be a source of alkali feldspar with highly efficient ice nucleation properties because rapid cooling rates make them less likely to form perthitic varieties of Kfs. In contrast, the Kfs reported from the rock record and discussed here is overwhelmingly composed of low(er) temperature, and slower forming polymorphs such as orthoclase and microcline, which are constituents of granite (*sensu stricto*) (see Table 1).

Timescales of potential impact

The actions of weathering, wash-out and burial must have returned Kfs to background levels after an upsurge in availability. Timescales depend upon regional land surface processes, which are difficult to estimate with enough accuracy to warrant comparison between events identified here. However, because modern annual dust recycling is estimated at c. 75% (Shao *et al.* 2011), meaning c. $<1 \text{ Pg a}^{-1}$ is transported to the oceans, a return to background levels of Kfs after being changed by major impact ejecta blankets may take place over thousands of years. These timescales are able to be resolved from some stratigraphic records (Galeotti *et al.* 2004).

What might be the effect of a 'Kfs-rich' atmospheric dust regime?

Increased ice nucleation efficiency would have different influences depending upon whether brighter clouds on average or shorter-lived clouds on average have more influence on the Earth's climate at the time of the event. Higher radiative transfer could lead to cooling, should the amount of cloud remain similar, or at least retain its role as the dominant albedo modulator. Shorter-lived clouds might decrease the average flux of water from oceans to the interiors of continents, and thereby also decrease the total amount of average cloud. Environments during times of super-continent tectonic regime would be expected to be more sensitive to this particular scenario of global hydrological change.

These two possible effects of increased ice nucleation efficiency on cloud properties and behaviour raise an intriguing set of tests that can be carried out when comparing similar-sized meteorite impact events in similar tectonic regimes, but different Kfs availability post-impact. Our study allows us to hypothesize that major environmental disruption via the hydrosphere is expected to have occurred in the years to thousands of years after a change to a high-Kfs regime, in addition to short-lived 'impact winter' effects expected via dust in the atmosphere. In contrast, similar-sized dust-

refreshing events without Kfs are expected to have influences only by those mechanisms attached to impact winter. Hydrological effects are tractable and quantifiable using observations from sedimentary strata, and magnitude and type of disruption may possibly be determined using the palaeontological record.

Conclusions

Major meteorite impact events in the past 600 myr have mobilized instantaneous dust volumes exceeding modern annual global dust emission by 1–3 orders of magnitude. Emissions from the resulting ejecta blankets probably dominated atmospheric mineralogy for hundreds to thousands of years after the impact.

A subset of these ejecta blankets were high in Kfs; they hold the greatest potential to change the global atmospheric ice nucleation regime so far recognized in geological history. Other ejecta blankets of similar size cannot be said to have changed the ice nucleation regime from background. This distinction provides the basis for assessing the impacts of direct v. indirect effects of mineral aerosol. Comparison with other data from stratigraphic records presents an opportunity to further understanding of links within the Earth system via cloud behaviour and properties.

Acknowledgements G. Osinski, L. Pittarello and H. J. Melosh are thanked for providing thoughtful reviews, which improved the paper. I. Fitzsimons is thanked for his editorial role

Funding M.P. thanks the AXA Research Fund and NERC (UK) (grant NE/M013561/1) for support.

Scientific editing by Ian Fitzsimons

References

- Andreae, M.O. 2007. Aerosols before pollution. *Science*, **315**, 50–51.
- Astitha, M., Lelieveld, J., Abdel Kader, M., Pozzer, A. & de Meij, A. 2012. Parameterization of dust emissions in the global atmospheric chemistry–climate model EMAC: impact of nudging and soil properties. *Atmospheric Chemistry and Physics*, **12**, 11057–11083, <https://doi.org/10.5194/acp-12-11057-2012>
- Atkinson, J.D., Murray, B.J. et al. 2013. The importance of feldspar for ice nucleation by mineral dust in mixed-phase clouds. *Nature*, **498**, 355–358, <https://doi.org/10.1038/nature12278>
- Booth, B.B.B., Harris, G.R., Murphy, J.M., House, J.I., Jones, C.D., Sexton, D. & Sitch, S. 2017. Narrowing the range of future climate projections using historical observations of atmospheric CO₂. *Journal of Climate*, **30**, 3039–3053, <https://doi.org/10.1175/jcli-d-16-0178.1>
- Bottomley, R., Grieve, R., York, D. & Masaitis, V. 1997. The age of the Popigai impact event and its relation to events at the Eocene/Oligocene boundary. *Nature*, **388**, 365–368, https://doi.org/http://www.nature.com/nature/journal/v388/n6640/supplinfo/388365a0_S1.html
- Boucher, O., Randall, D. et al. 2013. Clouds and aerosols. In: Stocker, T.F., Qin, D. et al. (eds) *Climate Change 2013: The Physical Science Basis. Contribution of Working Group 1 to the Fifth Assessment Report of the Intergovernmental Panel on Climate Change*. Cambridge University Press, Cambridge, 571–657.
- Bron, K.A. & Gostin, V. 2012. The Tookoonooka marine impact horizon, Australia: Sedimentary and petrologic evidence. *Meteoritics & Planetary Science*, **47**, 296–318, <https://doi.org/10.1111/j.1945-5100.2012.01330.x>
- Buseck, P.R. & Pósfai, M. 1999. Airborne minerals and related aerosol particles: Effects on climate and the environment. *Proceedings of the National Academy of Sciences of the USA*, **96**, 3372–3379.
- Buyce, M.R. & Friedman, G.M. 1975. Significance of authigenic K-feldspar in Cambrian–Ordovician carbonate rocks of the proto-Atlantic shelf in North America. *Journal of Sedimentary Research*, **45**, 808–821.
- Carpenter, B.N. & Carlson, R. 1992. *The Ames impact crater*. Oklahoma Geological Survey, Norman, Oklahoma.
- Carlsaw, K.S., Gordon, H., Hamilton, D.S., Johnson, J.S., Regayre, L.A., Yoshioka, M. & Pringle, K.J. 2017. Aerosols in the pre-industrial atmosphere. *Current Climate Change Reports*, **3**, 1–15, <https://doi.org/10.1007/s40641-017-0061-2>
- Christiansen, R.L. 2001. *The Quaternary and Pliocene Yellowstone Plateau Volcanic Field of Wyoming, Idaho, and Montana*. US Geological Survey, Professional Papers **729-G**.
- Cintala, M.J. & Grieve, R.A. 1998. Scaling impact melting and crater dimensions: Implications for the lunar cratering record. *Meteoritics & Planetary Science*, **33**, 889–912.
- Claquin, T., Schulz, M. & Balkanski, Y. 1999. Modeling the mineralogy of atmospheric dust sources. *Journal of Geophysical Research: Atmospheres*, **104**, 22243–22256.
- Collins, G.S., Melosh, H.J. & Marcus, R.A. 2005. Earth Impact Effects Program: A Web-based computer program for calculating the regional environmental consequences of a meteoroid impact on Earth. *Meteoritics & Planetary Science*, **40**, 817–840.
- Covey, C., Thompson, S.L., Weissman, P.R. & MacCracken, M.C. 1994. Global climatic effects of atmospheric dust from an asteroid or comet impact on Earth. *Global and Planetary Change*, **9**, 263–273.
- Croft, S. 1984. Scaling of complex craters. In: *Proceedings of [15th] Lunar and Planetary Science Conference*, Lunar and Planetary Institute, Houston Texas, 188–189.
- Darlington, V., Blenkinsop, T., Dirks, P., Salisbury, J. & Tomkins, A. 2016. The Lawn Hill annulus: An Ordovician meteorite impact into water-saturated dolomite. *Meteoritics & Planetary Science*, **51**, 2416–2440.
- Díaz-Hernández, J., Martín-Ramos, J. & López-Galindo, A. 2011. Quantitative analysis of mineral phases in atmospheric dust deposited in the south-eastern Iberian Peninsula. *Atmospheric Environment*, **45**, 3015–3024.
- Eriksson, P., Schreiber, U., Reczkó, B. & Snyman, C. 1994. Petrography and geochemistry of sandstones interbedded with the Rooiberg Felsite Group (Transvaal Sequence, South Africa): implications for provenance and tectonic setting. *Journal of Sedimentary Research*, **64**, 836–846.
- Eriksson, P.G., Banerjee, S. et al. 2013. Secular changes in sedimentation systems and sequence stratigraphy. *Gondwana Research*, **24**, 468–489, <https://doi.org/10.1016/j.gr.2012.09.008>
- Feldman, V., Sazonova, L., Mironov, Y.V., Kapustkina, I. & Ivanov, B. 1983. Circular structure Logancha as possible meteorite crater in basalts of the Tunguska syncline. In: *Proceedings of [14th] Lunar and Planetary Science Conference*, Lunar and Planetary Institute, Houston Texas, 191–192.
- Fel'dman, V.I., Sazonova, L.V. & Nozova, A.A. 1985. The structure and petrography of impactites of the Puchezh–Katunki astrobleme. *International Geology Review*, **27**, 68–77, <https://doi.org/10.1080/00206818509466391>
- Ferrière, L., Lubala, F.R., Osinski, G.R. & Kaseti, P.K. 2011. The newly confirmed Luizi impact structure, Democratic Republic of Congo – Insights into central uplift formation and post-impact erosion. *Geology*, **39**, 851–854.
- Floran, R.J., Grieve, R.A.F., Phinney, W.C., Warner, J.L., Simonds, C.H., Blanchard, D.P. & Dence, M.R. 1978. Manicouagan Impact Melt, Quebec, 1, Stratigraphy, petrology, and chemistry. *Journal of Geophysical Research: Solid Earth*, **83**, 2737–2759, <https://doi.org/10.1029/JB083iB06p02737>
- Folk, R.L. 1980. *Petrology of Sedimentary Rocks*. Hemphill, Tulsa, OK.
- French, B.M. 1998. *Traces of catastrophe: A handbook of shock-metamorphic effects in terrestrial meteorite impact structures*. LPI Contribution No. 954, Lunar and Planetary Institute, Houston, Texas, USA.
- Fuhrer, K., Wolff, E.W. & Johnsen, S.J. 1999. Timescales for dust variability in the Greenland Ice Core Project (GRIP) ice core in the last 100 000 years. *Journal of Geophysical Research: Atmospheres*, **104**, 31043–31052.
- Galeotti, S., Brinkhuis, H. & Huber, M. 2004. Records of post-Cretaceous–Tertiary boundary millennial-scale cooling from the western Tethys: A smoking gun for the impact-winter hypothesis? *Geology*, **32**, 529–532.
- Gieré, R. & Querol, X. 2010. Solid particulate matter in the atmosphere. *Elements*, **6**, 215–222.
- Glaccum, R.A. & Prospero, J.M. 1980. Saharan aerosols over the tropical North Atlantic – Mineralogy. *Marine Geology*, **37**, 295–321.
- Glikson, A. 1969. *Geology of the outer zone of the Gosses Bluff cryptoexplosion structure*. BMR Australia Record, **1969/42**, 30.
- Gostin, V.A. & Zbik, M. 1999. Petrology and microstructure of distal impact ejecta from the Flinders Ranges, Australia. *Meteoritics & Planetary Science*, **34**, 587–592.
- Gostin, V.A., Haines, P.W., Jenkins, R.J.F., Compston, W. & Williams, I.S. 1986. Impact ejecta horizon within Late Precambrian shales, Adelaide Geosyncline, South Australia. *Science*, **233**, 198–200, <https://doi.org/10.1126/science.233.4760.198>
- Grieve, R.A.F. & Floran, R.J. 1978. Manicouagan Impact Melt, Quebec 2. Chemical interrelations with basement and formational processes. *Journal of Geophysical Research: Solid Earth*, **83**, 2761–2771, <https://doi.org/10.1029/JB083iB06p02761>
- Grieve, R.A.F. & Head, J.W. 1983. The Manicouagan Impact Structure: An analysis of its original dimensions and form. *Journal of Geophysical Research: Solid Earth*, **88**, A807–A818, <https://doi.org/10.1029/JB088iB06p02760>
- Grieve, R.A., Therriault, A.M. & Kreis, L.K. 1998. Impact structures of the western sedimentary basin of North America: New discoveries and hydrocarbon resources. In: Christopher, J.E., Gilboy, C.F., Paterson, D.F. & Bend, S.L. (eds) *Eighth International Williston Basin Symposium*. Saskatchewan Geological Society, Special Publication, **13**, 189–201.
- Gurnis, M., Turner, M. et al. 2012. Plate tectonic reconstructions with continuously closing plates. *Computers & Geosciences*, **38**, 35–42.
- Gurov, E.P. & Koebel, C. 2004. Shocked rocks and impact glasses from the El'gygytgyn impact structure, Russia. *Meteoritics & Planetary Science*, **39**, 1495–1508.

- Gurov, E., Gurova, H., Rakitskaya, R. & Yamnichenko, A.Y. 1993. The Karakul depression in Pamirs: the first impact structure in Central Asia. In: *Proceedings of [24th] Lunar and Planetary Science Conference*. Lunar and Planetary Institute, Houston Texas, 591–592.
- Gurov, E.P., Kelley, S.P., Koeberl, C. & Dykan, N.I. 2006. Sediments and impact rocks filling the Bolysh impact crater. In: Cockell, C., Koeberl, C. & Gilmour, I. (eds) *Biological Processes Associated with Impact Events*. Springer, Berlin, 335–358.
- Gurov, E., Gurova, E., Chernenko, Y. & Yamnichenko, A. 2009. The Obolon impact structure, Ukraine, and its ejecta deposits. *Meteoritics & Planetary Science*, **44**, 389–404.
- Harper, C. 1981. *Geology of the Carswell structure, central part*. Saskatchewan Geological Survey, Regina, SK, Canada.
- Harrison, A.D., Whale, T.F. et al. 2016. Not all feldspar is equal: a survey of ice nucleating properties across the feldspar group of minerals. *Atmospheric Chemistry and Physics Discussions*, **2016**, 1–26, <https://doi.org/10.5194/acp-2016-136>
- Herbert, R.J., Murray, B.J., Dobbie, S.J. & Koop, T. 2015. Sensitivity of liquid clouds to homogeneous freezing parameterizations. *Geophysical Research Letters*, **42**, 1599–1605.
- Higgins, M. & Tait, L. 1990. A possible new impact structure near Lac de la Presqu'ile, Québec, Canada. *Meteoritics*, **25**, 235–236.
- Hofer, S., Tedstone, A.J., Fettweis, X. & Bamber, J.L. 2017. Decreasing cloud cover drives the recent mass loss on the Greenland Ice Sheet. *Science Advances*, **3**, <https://doi.org/10.1126/sciadv.1700584>
- Holsapple, K. 1993. The scaling of impact processes in planetary sciences. *Annual Review of Earth and Planetary Sciences*, **21**, 333–373.
- Holsapple, K.A. 2017. Craters from Explosions or Impacts, <http://keith.aa.washington.edu/craterdata/scaling/index.htm>.
- Hoose, C. & Möhler, O. 2012. Heterogeneous ice nucleation on atmospheric aerosols: a review of results from laboratory experiments. *Atmospheric Chemistry and Physics*, **12**, 9817–9854, <https://doi.org/10.5194/acp-12-9817-2012>
- Horton, J.W. & Izett, G.A. 2005. Chapter E: Crystalline-rock ejecta and shocked minerals of the Chesapeake Bay impact structure, USGS-NASA Langley core, Hampton, Virginia, with supplemental constraints on the age of impact. In: Horton, J.W., Powars, D.S. & Gohn, G.S. (eds) *Studies of the Chesapeake Bay impact structure: the USGS-NASA Langley corehole, Hampton, Virginia, and related coreholes and geophysical surveys*. Professional paper **1688**, U.S. Geological Survey, Reston, Virginia.
- Horton, J.W., Aleinikof, J.N., Kunk, M.J., Naeser, C.W. & Naeser, N.D. 2005. Chapter B: Petrography, structure, age, and thermal history of granitic coastal plain basement in the chesapeake bay impact structure, USGS-NASA langley core, Hampton, Virginia. In: Horton, J.W., Powars, D.S. & Gohn, G.S. (eds) *Studies of the Chesapeake Bay impact structure: the USGS-NASA Langley corehole, Hampton, Virginia, and related coreholes and geophysical surveys*. Professional paper **1688**. U.S. Geological Survey, Reston, Virginia.
- Horton, J.W., Gohn, G.S., Powars, D.S. & Edwards, L.E. 2007. Origin and emplacement of impactites in the Chesapeake Bay impact structure, Virginia, USA. In: Evans, K.R., Horton, J.W., Jr., King, D.T., Jr. & Morrow, J.R. (eds) *The Sedimentary Record of Meteorite Impacts*. Geological Society of America, Special Papers, **437**, 73–97, [https://doi.org/10.1130/2008.2437\(06\)](https://doi.org/10.1130/2008.2437(06))
- Horton, J.W., Gibson, R.L., Reimold, W.U., Wittmann, A., Gohn, G.S. & Edwards, L.E. 2009. Geologic columns for the ICDP-USGS Eyreville B core, Chesapeake Bay impact structure: Impactites and crystalline rocks, 1766 to 1096 m depth. In: Horton, J.W., Jr., Gibson, R.L., Reimold, W.U., Wittmann, A., Gohn, G.S. & Edwards, L.E. (eds) *The ICDP-USGS Deep Drilling Project in the Chesapeake Bay Impact Structure: Results from the Eyreville Core Holes*. Geological Society of America, Special Papers, **458**, 21–49, [https://doi.org/10.1130/2009.2458\(02\)](https://doi.org/10.1130/2009.2458(02))
- Hörz, F. 1982. Ejecta of the Ries Crater, Germany. In: Silver, L.T. & Schultz, P.H. (eds) *Geological Implications of Impacts of Large Asteroids and Comets on the Earth*. Geological Society of America, Special Papers, **190**, 39–56, <https://doi.org/10.1130/SPE190-p39>
- Hough, R., Lee, M. & Bevan, A. 2003. Characterization and significance of shocked quartz from the Woodleigh impact structure, Western Australia. *Meteoritics & Planetary Science*, **38**, 1341–1350.
- Izett, G., Masaitis, V., Shoemaker, E., Dalrymple, G. & Steiner, M. 1994. Eocene age of the Kamensk buried crater of Russia. In: *New developments regarding the KT event and other catastrophes in Earth history*. Houston, TX, 55.
- Jansa, L.F., Pe-Piper, G., Robertson, P.B. & Friedenreich, O. 1989. Montagnais: A submarine impact structure on the Scotian Shelf, eastern Canada. *Geological Society of America Bulletin*, **101**, 450–463, [https://doi.org/10.1130/0016-7606\(1989\)101<0450:masiso>2.3.co;2](https://doi.org/10.1130/0016-7606(1989)101<0450:masiso>2.3.co;2)
- Jeong, G.Y. 2008. Bulk and single-particle mineralogy of Asian dust and a comparison with its source soils. *Journal of Geophysical Research: Atmospheres*, **113**, D2, <https://doi.org/10.1029/2007JD008606>
- Jourdan, F., Renne, P. & Reimold, W. 2009. An appraisal of the ages of terrestrial impact structures. *Earth and Planetary Science Letters*, **286**, 1–13.
- Kandler, K., Schütz, L. et al. 2009. Size distribution, mass concentration, chemical and mineralogical composition and derived optical parameters of the boundary layer aerosol at Tinfou, Morocco, during SAMUM 2006. *Tellus B*, **61**, 32–50.
- Kandler, K., Schütz, L. et al. 2011. Ground-based off-line aerosol measurements at Praia, Cape Verde, during the Saharan Mineral Dust Experiment: microphysical properties and mineralogy. *Tellus B*, **63**, 459–474.
- Kelley, S. 2007. The geochronology of large igneous provinces, terrestrial impact craters, and their relationship to mass extinctions on Earth. *Journal of the Geological Society, London*, **164**, 923–936, <https://doi.org/10.1144/0016-76492007-026>
- Kenkmann, T., Afifi, A.M., Stewart, S.A., Poelchau, M.H., Cook, D.J. & Neville, A.S. 2015. Saqqar: A 34 km diameter impact structure in Saudi Arabia. *Meteoritics & Planetary Science*, **50**, 1925–1940, <https://doi.org/10.1111/maps.12555>
- Kettrup, B., Deutsch, A. & Masaitis, V.L. 2003. Homogeneous impact melts produced by a heterogeneous target?: Sr–Nd isotopic evidence from the Popigai crater, Russia. *Geochimica et Cosmochimica Acta*, **67**, 733–750, [https://doi.org/10.1016/S0016-7037\(02\)01143-2](https://doi.org/10.1016/S0016-7037(02)01143-2)
- Kiselev, A., Bachmann, F., Pedevilla, P., Cox, S.J., Michaelides, A., Gerthsen, D. & Leisner, T. 2017. Active sites in heterogeneous ice nucleation – the example of K-rich feldspars. *Science*, **355**, 367–371.
- Koeberl, C., Sharpton, V.L., Harrison, T.M., Sandwell, D., Murali, A.V. & Burke, K. 1990. The Kara/Ust-Kara twin impact structure; A large-scale impact event in the Late Cretaceous. In: Sharpton, V.L. & Ward, P.D. (eds) *Global catastrophes in Earth history: An interdisciplinary conference on impacts, volcanism, and mass mortality*. Geological Society of America, Special Papers, **247**, 233–238, <https://doi.org/10.1130/SPE247-p233>
- Koeberl, C., Armstrong, R.A. & Uwe Reimold, W. 1997. Morokweng, South Africa: A large impact structure of Jurassic–Cretaceous boundary age. *Geology*, **25**, 731–734, [https://doi.org/10.1130/0091-7613\(1997\)025<731:msaal>2.3.co;2](https://doi.org/10.1130/0091-7613(1997)025<731:msaal>2.3.co;2)
- Komor, S.C. & Valley, J.W. 1990. Deep drilling at the Siljan Ring impact structure: oxygen-isotope geochemistry of granite. *Contributions to Mineralogy and Petrology*, **105**, 516–532, <https://doi.org/10.1007/bf00302492>
- Komurcu, M., Storelvmo, T. et al. 2014. Intercomparison of the cloud water phase among global climate models. *Journal of Geophysical Research: Atmospheres*, **119**, 3372–3400, <https://doi.org/10.1002/2013JD021119>
- Koop, T. & Murray, B.J. 2016. A physically constrained classical description of the homogeneous nucleation of ice in water. *Journal of Chemical Physics*, **145**, 211915.
- Kraut, F. & French, B.M. 1971. The Rochechouart meteorite impact structure, France: Preliminary geological results. *Journal of Geophysical Research*, **76**, 5407–5413.
- Lambert, P. 2010. Target and impact deposits at Rochechouart impact structure, France. In: Gibson, R.L. & Reimold, W.U. (eds) *Large Meteorite Impacts and Planetary Evolution IV*. Geological Society of America, Special Papers, **465**, 509–541, [https://doi.org/10.1130/2010.2465\(25\)](https://doi.org/10.1130/2010.2465(25))
- Lambert, F., Delmonte, B. et al. 2008. Dust–climate couplings over the past 800 000 years from the EPICA Dome C ice core. *Nature*, **452**, 616–619.
- Langmann, B. 2014. On the role of climate forcing by volcanic sulphate and volcanic ash. *Advances in Meteorology*, **2014**, 17, <https://doi.org/10.1155/2014/340123>
- Lehnert, O., Meinhold, G. et al. 2012. New Ordovician–Silurian drill cores from the Siljan impact structure in central Sweden: an integral part of the Swedish Deep Drilling Program. *GFF*, **134**, 87–98.
- Lohmann, U. & Feichter, J. 2005. Global indirect aerosol effects: a review. *Atmospheric Chemistry and Physics*, **5**, 715–737.
- Macdonald, F., Wingate, M. & Mitchell, K. 2005. Geology and age of the Glikson impact structure, Western Australia. *Australian Journal of Earth Sciences*, **52**, 641–651.
- Machado, R., Lana, C., Stevens, G., Reimold, W. & McDonald, I. 2009. Generation, mobilization and crystallization of impact-induced alkali-rich melts in granitic target rocks: Evidence from the Araguainha impact structure, central Brazil. *Geochimica et Cosmochimica Acta*, **73**, 7183–7201.
- Mahowald, N., Albani, S., Kok, J.F., Engelstaeder, S., Scanza, R., Ward, D.S. & Flanner, M.G. 2014. The size distribution of desert dust aerosols and its impact on the Earth system. *Aeolian Research*, **15**, 53–71, <https://doi.org/10.1016/j.aeolia.2013.09.002>
- Marchand, M. & Crocket, J.H. 1977. Sr isotopes and trace element geochemistry of the impact melt and target rocks at the Mistastin Lake crater, Labrador. *Geochimica et Cosmochimica Acta*, **41**, 1487–1495, [https://doi.org/10.1016/0016-7037\(77\)90253-8](https://doi.org/10.1016/0016-7037(77)90253-8)
- Marticorena, B. 2014. Dust production mechanisms. In: Knippertz, P. & Stuut, J.-B.W. (eds) *Mineral Dust: A Key Player in the Earth System*. Springer, Dordrecht, 93–120.
- Martin, A. 1969. Possible impact structure in southern Cyrenaica, Libya. *Nature*, **223**, 940–941.
- Masaitis, V.L. 2003. Obscure-bedded ejecta facies from the Popigai impact structure, Siberia: lithological features and mode of origin. In: Koeberl, C. & Martínez-Ruiz, F.C. (eds) *Impact Markers in the Stratigraphic Record*. Springer, Berlin, 137–162.
- Masaitis, V. & Mashchak, M. 1990. Puchezh–Katunki astrobleme: structure of central uplift and transformation of composing rocks. *Meteoritics*, **25**, 383.
- Mashchak, M.S. 1991. Geologic setting in Kara and Ust’-Kara at the time of formation of the impact craters. *International Geology Review*, **33**, 423–432, <https://doi.org/10.1080/00206819109465700>
- Matthews, K.J., Maloney, K.T., Zahirovic, S., Williams, S.E., Seton, M. & Müller, R.D. 2016. Global plate boundary evolution and kinematics since the late Paleozoic. *Global and Planetary Change*, **146**, 226–250.
- Melles, M., Brigham-Grette, J. et al. 2011. The Lake El'gygytgyn Scientific Drilling Project – conquering Arctic challenges through continental drilling. *Scientific Drilling*, **11**, 29–40.

- Melosh, H.J. 1989. *Impact Cratering: A Geologic Process*. Oxford Monographs on Geology and Geophysics, **11**. Oxford University Press, Oxford.
- Molak, B. 2001. *Petrographic, mineralogical and lithogeochemical study of core from three drillholes into the Steen River Structure, northern Alberta*. Alberta Geological Survey, Edmonton, Canada.
- Morgan, J., Warner, M. & Grieve, R. 2002. Geophysical constraints on the size and structure of the Chicxulub impact crater. In: Koeberl, C. & MacLeod, K.G. (eds) *Catastrophic Events and Mass Extinctions: Impacts and Beyond*. Geological Society of America, Special Papers, **356**, 39–46.
- Morgan, J.V., Gulick, S.P.S. et al. 2016. The formation of peak rings in large impact craters. *Science*, **354**, 878–882, <https://doi.org/10.1126/science.aah6561>
- Morrow, J.R., Sandberg, C.A., Malkowski, K. & Joachimski, M.M. 2009. Carbon isotope chemostratigraphy and precise dating of middle Frasnian (lower Upper Devonian) Alamo Breccia, Nevada, USA. *Palaeogeography, Palaeoclimatology, Palaeoecology*, **282**, 105–118, <https://doi.org/https://doi.org/10.1016/j.palaeo.2009.08.016>
- Murray, B., O'Sullivan, D., Atkinson, J. & Webb, M. 2012. Ice nucleation by particles immersed in supercooled cloud droplets. *Chemical Society Reviews*, **41**, 6519–6554.
- Napier, W.M. 2006. Evidence for cometary bombardment episodes. *Monthly Notices of the Royal Astronomical Society*, **366**, 977–982.
- Nenes, A., Murray, B. & Bougiatioti, A. 2014. Mineral dust and its microphysical interactions with clouds. In: Knippertz, P. & Stut, J.-B.W. (eds) *Mineral Dust: A Key Player in the Earth System*. Springer, Berlin, 287–325.
- O'Keefe, J.D. & Ahrens, T.J. 1985. Impact and explosion crater ejecta, fragment size, and velocity. *Icarus*, **62**, 328–338.
- Osinski, G.R. 2004. Impact melt rocks from the Ries structure, Germany: an origin as impact melt flows? *Earth and Planetary Science Letters*, **226**, 529–543, <https://doi.org/https://doi.org/10.1016/j.epsl.2004.08.012>
- Osinski, G.R. & Ferrière, L. 2016. Shatter cones(Mis) understood? *Science Advances*, **2**, e1600616.
- Osinski, G.R., Spray, J.G. & Grieve, R.A.F. 2007. Impact melting in sedimentary target rocks: An assessment. In: Evans, K.R., Horton, J.W., Jr., King, D.T., Jr. & Morrow, J.R. (eds) *The Sedimentary Record of Meteorite Impacts*. Geological Society of America, Special Papers, **437**, 1–18, [https://doi.org/10.1130/2008.2437\(01\)](https://doi.org/10.1130/2008.2437(01))
- Osinski, G., Grieve, R., Collins, G., Marion, C. & Sylvester, P. 2008. The effect of target lithology on the products of impact melting. *Meteoritics & Planetary Science*, **43**, 1939–1954.
- Osinski, G.R., Tornabene, L.L. & Grieve, R.A. 2011. Impact ejecta emplacement on terrestrial planets. *Earth and Planetary Science Letters*, **310**, 167–181.
- Osinski, G.R., Grieve, R.A.F. & Tornabene, L.L. 2012. Excavation and impact ejecta emplacement. In: Osinski, G.R. & Pierazzo, E. (eds) *Impact Cratering: Processes and Products*. Wiley, Chichester, 43–59.
- Pankhurst, M.J. 2017. Atmospheric K-feldspar as a potential climate modulating agent through geologic time. *Geology*, <https://doi.org/10.1130/g38684.1>
- Pankhurst, M.J., Schaefer, B.F. & Betts, P.G. 2011a. Geodynamics of rapid voluminous felsic magmatism through time. *Lithos*, **123**, 92–101.
- Pankhurst, M.J., Schaefer, B.F., Betts, P.G., Phillips, N. & Hand, M. 2011b. A Mesoproterozoic continental flood rhyolite province, the Gawler Ranges, Australia: the end member example of the Large Igneous Province clan. *Solid Earth*, **2**, 1–9.
- Pankhurst, M.J., Schaefer, B.F., Turner, S.P., Argles, T. & Wade, C.E. 2013. The source of A-type magmas in two contrasting settings: U-Pb, Lu-Hf and Re-Os isotopic constraints. *Chemical Geology*, **351**, 175–194, <https://doi.org/https://doi.org/10.1016/j.chemgeo.2013.05.010>
- Parsons, I., Gerald, J.D.F. & Lee, M.R. 2015. Routine characterization and interpretation of complex alkali feldspar intergrowths. *American Mineralogist*, **100**, 1277–1303.
- PASSC. 2017. Earth Impact Database. Planetary and Space Science Center, University of New Brunswick, Fredericton, <http://www.unb.ca/passc/ImpactDatabase/>
- Peckhaus, A., Kiselev, A., Hiron, T., Ebert, M. & Leisner, T. 2016. A comparative study of K-rich and Na/Ca-rich feldspar ice nucleating particles in a nanoliter droplet freezing assay. *Atmospheric Chemistry and Physics Discussions*, **2016**, 1–43, <https://doi.org/10.5194/acp-2016-72>
- Pedevilla, P., Cox, S.J., Slater, B. & Michaelides, A. 2016. Can ice-like structures form on non-ice-like substrates? The example of the K-feldspar microcline. *Journal of Physical Chemistry C*, **120**, 6704–6713, <https://doi.org/10.1021/acs.jpcc.6b01155>
- Pinto, J.A. & Warne, J.E. 2007. Alamo Event, Nevada: Crater stratigraphy and impact breccia realms. In: Evans, K.R., Horton, J.W., Jr., King, D.T., Jr. & Morrow, J.R. (eds) *The Sedimentary Record of Meteorite Impacts*. Geological Society of America Special Papers, **437**, 99–137.
- Pipping, F. & Lehtinen, M. 1992. Geology, stratigraphy and structure of the Lappajärvi meteorite crater, western Finland: preliminary results of deep drilling. *Tectonophysics*, **216**, 91–97.
- Pittarello, L. & Koeberl, C. 2013a. Clast size distribution and quantitative petrography of shocked and unshocked rocks from the El'gygytgyn impact structure. *Meteoritics & Planetary Science*, **48**, 1325–1338, <https://doi.org/https://doi.org/10.1111/maps.12070>
- Pittarello, L. & Koeberl, C. 2013b. Petrography of impact glasses and melt breccias from the El'gygytgyn impact structure, Russia. *Meteoritics & Planetary Science*, **48**, 1236–1250, <https://doi.org/https://doi.org/10.1111/maps.12048>
- Prospero, J., Glaccum, R. & Nees, R. 1981. Atmospheric transport of soil dust from Africa to South America. *Nature*, **289**, 570–572.
- Rasband, W.S. 2015. *ImageJ*. 1997–2015. US National Institutes of Health, Bethesda, MD.
- Reagan, M.K., Foster, C.T., Bell, M.S. & Anderson, R.R. 1996. Preferential feldspar comminution in impact melt breccias from the M-1 core of the Manson impact structure. In: Koeberl, C. & Anderson, R.R. (eds) *The Manson Impact Structure, Iowa: Anatomy of an Impact Crater*. Geological Society of America, Special Papers, **302**, 235–243, <https://doi.org/10.1130/0-8137-2302-7.235>
- Reimold, W. 1982. The Lappajärvi meteorite crater, Finland: petrography, Rb-Sr, major and trace element geochemistry of the impact melt and basement rocks. *Geochimica et Cosmochimica Acta*, **46**, 1203–1225.
- Reimold, W.U. & Koeberl, C. 2014. Impact structures in Africa: A review. *Journal of African Earth Sciences*, **93**, 57–175.
- Reimold, W., Barr, J., Grieve, R. & Durheim, R. 1990. Geochemistry of the melt and country rocks of the Lake St. Martin impact structure, Manitoba, Canada. *Geochimica et Cosmochimica Acta*, **54**, 2093–2111.
- Reimold, W.U., Armstrong, R.A. & Koeberl, C. 2002. A deep drillcore from the Morokweng impact structure, South Africa: petrography, geochemistry, and constraints on the crater size. *Earth and Planetary Science Letters*, **201**, 221–232.
- Robertson, P.B. 1975. Zones of shock metamorphism at the Charlevoix impact structure, Quebec. *Geological Society of America Bulletin*, **86**, 1630–1638, [https://doi.org/10.1130/0013-7606\(1975\)86<1630:zomat>2.0.co;2](https://doi.org/10.1130/0013-7606(1975)86<1630:zomat>2.0.co;2)
- Robertson, P. & Sweeney, J. 1983. Haughton impact structure: Structural and morphological aspects. *Canadian Journal of Earth Sciences*, **20**, 1134–1151.
- Rozen, O. 1990. Two types of crust in the Anabar shield. *International Geology Review*, **32**, 551–564.
- Salisbury, J.A., Tomkins, A.G. & Schaefer, B.F. 2008. New insights into the size and timing of the Lawn Hill impact structure: relationship to the Century Zn-Pb deposit. *Australian Journal of Earth Sciences*, **55**, 587–603, <https://doi.org/10.1080/08120090801888677>
- Scheuvens, D., Schütz, L., Kandler, K., Ebert, M. & Weinbruch, S. 2013. Bulk composition of northern African dust and its source sediments – A compilation. *Earth-Science Reviews*, **116**, 170–194.
- Schmidt, A., Ostro, B., Carslaw, K.S., Wilson, M., Thordarson, T., Mann, G.W. & Simmons, A.J. 2011. Excess mortality in Europe following a future Laki-style Icelandic eruption. *Proceedings of the National Academy of Sciences of the USA*, **108**, 15710–15715, <https://doi.org/10.1073/pnas.1108569108>
- Schmieder, M., Schwarz, W.H., Trieloff, M., Tohver, E., Buchner, E., Hopp, J. & Osinski, G.R. 2015. New ^{40}Ar / ^{39}Ar dating of the Clearwater Lake impact structures (Québec, Canada) – Not the binary asteroid impact it seems? *Geochimica et Cosmochimica Acta*, **148**, 304–324, <https://doi.org/https://doi.org/10.1016/j.gca.2014.09.037>
- Scotese, C. 2016. PALEOMAP PaleoAtlas for GPlates and the PaleoData Plotter Program. PALEOMAP Project. http://www.earthbyte.org/paleomap_paleoatlas-for-gplates/ [last accessed March 2018].
- Shao, Y., Wyrwoll, K.-H. et al. 2011. Dust cycle: An emerging core theme in Earth system science. *Aeolian Research*, **2**, 181–204, <https://doi.org/https://doi.org/10.1016/j.aeolia.2011.02.001>
- Sharpton, V.L., Dressler, B.O., Herrick, R.R., Schnieders, B. & Scott, J. 1996. New constraints on the Slate Islands impact structure, Ontario, Canada. *Geology*, **24**, 851–854.
- Sherlock, S.C., Kelley, S.P., Parnell, J., Green, P., Lee, P., Osinski, G.R. & Cockell, C.S. 2005. Re-evaluating the age of the Haughton impact event. *Meteoritics & Planetary Science*, **40**, 1777–1787.
- Shields, G.A., Carden, G.A., Veizer, J., Meidla, T., Rong, J.-Y. & Li, R.-Y. 2003. Sr, C, and O isotope geochemistry of Ordovician brachiopods: A major isotopic event around the Middle–Late Ordovician transition. *Geochimica et Cosmochimica Acta*, **67**, 2005–2025.
- Siirola, J. & Schmid, R. 2007. *Recommendations by the IUGS Subcommission on the Systematics of Metamorphic Rocks: List of mineral abbreviations*. Web version 01.02.07, www.bgs.ac.uk/scmr/home.html.
- Silva, D., Lana, C. & de Souza Filho, C.R. 2016. Petrographic and geochemical characterization of the granitic rocks of the Araguainha impact crater, Brazil. *Meteoritics & Planetary Science*, **51**, 443–467, <https://doi.org/10.1111/maps.12601>
- Simonds, C., Phinney, W., McGee, P. & Cochran, A. 1978. West Clearwater, Quebec impact structure. I – Field geology, structure and bulk chemistry. II – Petrology. In: *[9th] Lunar and Planetary Science Conference Proceedings*, Lunar and Planetary Institute, Houston Texas, 2633–2693.
- Smith, D.B., Cannon, W.F., Woodruff, L.G., Solano, F. & Ellefsen, K.J. 2014. *Geochemical and mineralogical maps for soils of the conterminous United States*. US Geological Survey, Report, 2331–1258.
- Spray, J.G., Kelley, S.P. & Rowley, D.B. 1998. Evidence for a late Triassic multiple impact event on Earth. *Nature*, **392**, 171–173.
- Spray, J.G., Thompson, L.M., Biren, M.B. & O'Connell-Cooper, C. 2010. The Manicouagan impact structure as a terrestrial analogue site for lunar and martian planetary science. *Planetary and Space Science*, **58**, 538–551.
- Stinnesbeck, W., Keller, G., Adatte, T., Harting, M., Stüben, D., Istrate, G. & Kramar, U. 2004. Yaxcopoil-1 and the Chicxulub impact. *International Journal of Earth Sciences*, **93**, 1042–1065.
- Stocker, T.F. 2014. *Climate Change 2013: the Physical Science Basis: Working Group I Contribution to the Fifth Assessment Report of the Intergovernmental Panel on Climate Change*. Cambridge University Press, Cambridge.

- Stöffler, D., Artemieva, N., Pierazzo, E. & Ivanov, B. 2001. Ries crater, Germany: Geology and numerical modeling of impact cratering. *Meteoritics & Planetary Science Supplement*, **36**, A199.
- Storelvmo, T. 2017. Aerosol effects on climate via mixed-phase and ice clouds. *Annual Review of Earth and Planetary Sciences*, **45**, 199–222.
- Storelvmo, T., Hoose, C. & Eriksson, P. 2011. Global modeling of mixed-phase clouds: The albedo and lifetime effects of aerosols. *Journal of Geophysical Research: Atmospheres*, **116**, <https://doi.org/10.1029/2010JD014724>
- Strekelsen, A. 1974. Classification and nomenclature of plutonic rocks recommendations of the IUGS Subcommission on the Systematics of Igneous Rocks. *Geologische Rundschau*, **63**, 773–786.
- Svensson, N.-B. 1968. The Dellen Lakes, a probable meteorite impact in Central Sweden. *GFF*, **90**, 314–316, <https://doi.org/10.1080/11035896809451894>
- Tan, I., Storelvmo, T. & Zelinka, M.D. 2016. Observational constraints on mixed-phase clouds imply higher climate sensitivity. *Science*, **352**, 224–227.
- Taylor, S.R. & McLennan, S.M. 1995. The geochemical evolution of the continental crust. *Reviews in Geophysics*, **33**, 241–265.
- Textor, C., Schulz, M. et al. 2006. Analysis and quantification of the diversities of aerosol life cycles within AeroCom. *Atmospheric Chemistry and Physics*, **6**, 1777–1813.
- Thackrey, S., Walkden, G., Indares, A., Horstwood, M., Kelley, S. & Parrish, R. 2009. The use of heavy mineral correlation for determining the source of impact ejecta: A Manicouagan distal ejecta case study. *Earth and Planetary Science Letters*, **285**, 163–172, <https://doi.org/https://doi.org/10.1016/j.epsl.2009.06.010>
- Tohver, E., Lana, C. et al. 2012. Geochronological constraints on the age of a Permo-Triassic impact event: U–Pb and $^{40}\text{Ar}/^{39}\text{Ar}$ results for the 40 km Araguainha structure of central Brazil. *Geochimica et Cosmochimica Acta*, **86**, 214–227, <https://doi.org/https://doi.org/10.1016/j.gca.2012.03.005>
- Torsvik, T.H., Van der Voo, R. et al. 2012. Phanerozoic polar wander, palaeogeography and dynamics. *Earth-Science Reviews*, **114**, 325–368.
- Trela, W., Bąk, E. & Pańczyk, M. 2018. Upper Ordovician and Silurian ash beds in the Holy Cross Mountains, Poland: preservation in mudrock facies and relation to atmospheric circulation in the Southern Hemisphere. *Journal of the Geological Society, London*, **175**, 352–360, <https://doi.org/10.1144/jgs2017-026>
- Trepmann, C.A., Götte, T. & Spray, J.G. 2005. Impact-related Ca-metasomatism in crystalline target-rocks from the Charlevoix structure, Quebec, Canada. *Canadian Mineralogist*, **43**, 553–567.
- Trieloff, M., Deutsch, A. & Jessberger, E.K. 1998. The age of the Kara impact structure, Russia. *Meteoritics & Planetary Science*, **33**, 361–372, <https://doi.org/10.1111/j.1945-5100.1998.tb01640.x>
- Tsikalas, F., Gudlaugsson, S.T. & Faleide, J.I. 1998. The anatomy of a buried complex impact structure: The Mjølnir Structure, Barents Sea. *Journal of Geophysical Research: Solid Earth*, **103**, 30469–30483.
- Vali, G., DeMott, P.J., Möhler, O. & Whale, T.F. 2015. A proposal for ice nucleation terminology. *Atmospheric Chemistry and Physics*, **15**, 10263–10270, <https://doi.org/10.5194/acp-15-10263-2015>
- Vallelonga, P. & Svensson, A. 2014. Ice core archives of mineral dust. In: Knippertz, P. & Stut, J.-B.W. (eds) *Mineral Dust: A Key Player in the Earth System*. Springer, Berlin, 463–485.
- Hinsbergen, D.J., de Groot, L.V. et al. 2015. A paleolatitude calculator for paleoclimate studies. *PloS one*, **10**, e0126946.
- Vergara-Temprado, J., Miltenberger, A.K. et al. 2018. Strong control of Southern Ocean cloud reflectivity by ice-nucleating particles. *Proceedings of the National Academy of Sciences of the USA*, **115**, 2687–2692, <https://doi.org/10.1073/pnas.1721627115>
- Walkden, G. & Parker, J. 2008. The biotic effects of large bolide impacts: size v. time and place. *International Journal of Astrobiology*, **7**, 209–215.
- Ward, W., Keller, G., Stinesbeck, W. & Adatte, T. 1995. Yucatán subsurface stratigraphy: Implications and constraints for the Chicxulub impact. *Geology*, **23**, 873–876.
- Whale, T.F., Holden, M.A., Kulak, A.N., Kim, Y.-Y., Meldrum, F.C., Christenson, H.K. & Murray, B.J. 2017. The role of phase separation and related topography in the exceptional ice-nucleating ability of alkali feldspars. *Physical Chemistry Chemical Physics*, **19**, 31186–31193.
- White, A.F., Bullen, T.D., Schulz, M.S., Blum, A.E., Huntington, T.G. & Peters, N.E. 2001. Differential rates of feldspar weathering in granitic regoliths. *Geochimica et Cosmochimica Acta*, **65**, 847–869, [https://doi.org/10.1016/S0016-7037\(00\)00577-9](https://doi.org/10.1016/S0016-7037(00)00577-9)
- Whitney, D.L. & Evans, B.W. 2010. Abbreviations for names of rock-forming minerals. *American Mineralogist*, **95**, 185–187.
- Williams, G.E. 1986. The Acraman Impact Structure: source of ejecta in Late Precambrian shales, South Australia. *Science*, **233**, 200–203, <https://doi.org/10.1126/science.233.4760.200>
- Wolfe, A.P., Reyes, A.V. et al. 2017. Middle Eocene CO₂ and climate reconstructed from the sediment fill of a subarctic kimberlite maar. *Geology*, **45**, 619–622, <https://doi.org/10.1130/G39002.1>
- Wood, J.D. 2013. *Sedimentological characterization and regional palaeoenvironmental implications of the Messak Fm, SW Libya*. PhD thesis, University of Manchester.
- Xie, X., Zhang, H., Liu, X., Peng, Y. & Liu, Y. 2017. Sensitivity study of cloud parameterizations with relative dispersion in CAM5.1: impacts on aerosol indirect effects. *Atmospheric Chemistry and Physics*, **17**, 5877–5892, <https://doi.org/10.5194/acp-17-5877-2017>
- Yabushita, S. 2002. On the periodicity hypothesis of the ages of large impact craters. *Monthly Notices of the Royal Astronomical Society*, **334**, 369–373.
- Yang, P., Liou, K.-N., Bi, L., Liu, C., Yi, B. & Baum, B.A. 2015. On the radiative properties of ice clouds: Light scattering, remote sensing, and radiation parameterization. *Advances in Atmospheric Sciences*, **32**, 32–63.
- Young, K.E., van Soest, M.C., Hodges, K.V., Watson, E.B., Adams, B.A. & Lee, P. 2013. Impact thermochronology and the age of Haughton impact structure, Canada. *Geophysical Research Letters*, **40**, 3836–3840, <https://doi.org/10.1002/grl.50745>
- Zhao, W., Balsam, W., Williams, E., Long, X. & Ji, J. 2018. Sr–Nd–Hf isotopic fingerprinting of transatlantic dust derived from North Africa. *Earth and Planetary Science Letters*, **486**, 23–31, <https://doi.org/https://doi.org/10.1016/j.epsl.2018.01.004>
- Zolles, T., Burkart, J., Häusler, T., Pummer, B., Hitzenberger, R. & Grothe, H. 2015. Identification of ice nucleation active sites on feldspar dust particles. *Journal of Physical Chemistry A*, **119**, 2692–2700.